Università degli Studi di Urbino Carlo Bo

Department of Pure and Applied Sciences

Ph.D. PROGRAMME IN: Basic Sciences and Applications

CURRICULUM: Chemical and Pharmaceutical Sciences

CYCLE XXXIV

THE REVOLUTIONARY TECHNOLOGY OF 3D PRINTING IN THE PHARMACEUTICAL FIELD

ACADEMIC DISCIPLINE: CHIM/09

Coordinator: Chiarissimo Prof. Alessandro Bogliolo

Supervisor: Prof. Luca Casettari

Ph.D. student: Mattia Tiboni

ACADEMIC YEAR
2020/2021

DECLARATION

This thesis describes research conducted in the School of Pharmacy, University of Urbino Carlo Bo from November 2018 to October 2021 under the supervision of Professor Luca Casettari. I, Mattia Tiboni certify that the research described is original and that I have written all the text herein and have clearly indicated by suitable citation any part of this dissertation that has already appeared in publication.

Chi più in alto sale, più lontano vede.
Chi più lontano vede, più a lungo sogna.

-Walter Bonatti-

TABLE OF CONTENTS

ABSTRACT

From when the first 3D printing technology was patented, this manufacturing field has grown exponentially developing new techniques and inventing innovative applications. During the last decade, the interest in its usage for pharmaceutical-related purposes raise dramatically.

3D printing has been explored to produce pharmaceutical forms, medical devices, manufacturing devices, and analytical devices.

In this thesis, the results of the research conducted with the application of 3D printing during my PhD programme has been presented.

As medical device, we were able to efficiently produce a 3D printed intravaginal ring loaded with clotrimazole. This ring showed a sustained release and an efficient killing activity against *C. Albicans*, the pathogen causing vaginal candidiasis.

Then, as manufacturing devices, we developed 3D printed microfluidic devices firstly using polylactic acid and then polypropylene. Using them, we manufactured lipid and polymer-based nanocarriers in a controllable and tunable manner encapsulating glycyrrhetinic acid, and cannabidiol. These devices resulted resistant to the manufacturing process with a very lower overall cost compared to commercially available microfluidic systems and with the possibility of quick personalization based on the user needs.

Finally, as analytical device, we developed a 3D printed vertical diffusion cell or Franz cell that can be efficiently used instead of glass ones to evaluate drug release and/or permeation.

This thesis provides new insights on the use of 3D printing for pharmaceutical applications, supporting the idea that in the close future 3D printing will be used for the formulation of personalized medicines in pharmacies and that this technology will help the diffusion of personalized and low-cost manufacturing and analytical devices in research laboratories.

IMPACT STATEMENT

Since 1986, the year in which the first 3D printing technology has been patented by Chuck Hull, this manufacturing approach has grown exponentially in many fields developing new techniques and applications. During the last few years, its usage has arrived in the pharmaceutical field where it starts a real hype.

Rapidity, flexibility, and the possibility of personalization intrinsic in 3D printing helped to revolutionise the pharmaceutical field.

This thesis aimed to investigate the potential applications of 3D printing in the production of pharmaceutical forms but also personalized manufacturing and analytical devices. In the present work, a 3D printed antifungal intravaginal ring has been developed as medical device, 3D printed microfluidic devices have been produced to be effectively used to manufacture nanocarriers, and a 3D printed vertical diffusion cell have been created to be used as an alternative to the common glass-based ones.

Thus, this work wants to broaden the knowledge about 3D printed personalized dosage forms and moreover, it aims to broaden the accessibility to microfluidics as manufacturing technology for the scalable production of nanocarriers already from the basic research steps into research laboratories.

This approach has the potential to widen accessibility further by eliminating the design barrier in addition to the fabrication barrier largely limiting access to microfluidic technology at present.

PREFACE

Over the years, innovative technologies have been always introduced in the pharmaceutical field to ameliorate the quality of the final products. Among these technologies, during the last few years, additive manufacturing (AM) has taken space in the field as an alternative to conventional production techniques. According to its definition (ISO/ASTM 52900:2015), AM includes all manufacturing methods in which the final 3D object is built by sequential addition of material as opposed to traditional subtractive approaches. AM could be included in the set of rapid prototyping techniques that naturally appear as a fundamental tool in research and development area thanks to the reduction of both time and costs in the early stage of a novel manufacturing concept [1].

Usually, to reach the desired 3D object, this must be digitally rendered using a computer-aided design (CAD) software and then exported in rapid prototyping stereolithography (.stl) file format. This format transforms the geometries and sizes of the parts into triangles that together make up the surface of the designed 3D structure [2]. Then, the last step is to process the .stl file by creating digitally sliced layers of the model that can be subsequentially deposited by the 3D printer.

Since 1986, the year in which the first 3D printing (3DP) technology has been patented, many different 3DP technologies have been introduced in the market [3] and among them, one in particular, known as fused deposition modeling (FDM), has created an escalation in the pharmaceutical field [4].

The FDM technique relies on the extrusion process using a filament obtained from a thermoplastic material that is driven, through a geared system into a heated nozzle in the printing head. Here, becoming softer, it can be deposed layer by layer over the 3D printer building plate. By optimizing the printing parameters, the user can obtain perfectly fused layers in the final object.

The printing filaments can be obtained ready to be printed in the market or created using hot melt extrusion starting from pellets of the desired thermoplastic polymer. The main strength of rapid prototyping and 3D printing is the possibility to create personalized objects [5]. It results true also for pharmaceutical applications during the production of medicines [6], medical devices [7], manufacturing devices [8–10], and analytical devices [11]. All of them can be personalized based on the patient or user’s needs.

During the last five years, thanks to FDM, different personalized dosage forms have been developed and characterized such as hollow structures and tablets for oral administration with different shapes [4,12]. Moreover, the oral forms can be composed of a single active molecule or more than one by layering different materials. These changes that can be easily made thanks to rapid prototyping and then 3D printing can affect the drug release patterns to obtain for example a controlled or immediate release [12]. Among 3DP drug delivery strategies, other systems for parenteral, topical, vaginal, rectal, and intravesical administration have been created. Among them, it is worthy to mention the development of drug-eluting stents intended to keep vessels open [13], scaffolds mainly working as substitutes for human bone parts with the ability of eluting drugs [14], implants for prolonged drug release with different shapes and drug release patterns [15–17]. Moreover, patches and microneedles have been printed using FDM with the possibility to design them for perfect adherence to the body surface of the patients [18,19]. Other strategies were the development of vaginal and intravesical insert to obtain a localized and prolonged drug delivery applying also the so-called 4D printing in which shape-memory materials are used to change their form after external stimuli such as the change of pH, temperature, or hydration [20–22].

Nevertheless, this field is growing and innovative ideas are coming from researchers all around the world.

In this thesis, the FDM technique has been used and its application possibilities have been explored by producing a medical device, two manufacturing devices (*i.e.*, microfluidic chips), and an analytical device.

As medical device, an intravaginal ring IVR was developed and evaluated as an antifungal medication (*Part I*) [7]. To do so, clotrimazole was integrated with thermoplastic polyurethane (TPU) using hot melt extrusion to produce the printing filament loaded with the drug (*i.e.*, 2% and 10 % w/w).

IVRs are flexible devices made with biocompatible polymers that possess controlled drug release and good patient compliance due to a single application for a long period of treatment [20]. The marketed IVRs are used for hormone therapy or contraception [23] and in this work it has been explored its applicability for antifungal therapy as proof of concept.

Clotrimazole was selected as a model antifungal drug since it is considered a first-line treatment in *C. Albicans* infections acting as an ergosterol synthesis inhibitor [24]. This drug is commonly administered locally with conventional formulations such as creams, emulsions, gels, or orally with tablets [25] on a daily basis. So, the one-time application through an IVR has the potential to increase the patient's adherence to the therapy. Moreover, thanks to the 3DP manufacturing approach, the final product can be personalized in terms of dosage and shape based on patient needs [20,26]. As biocompatible polymer, TPU was selected thanks to its elasticity, flexibility, and high potential to provide sustained drug release as requested for IVRs [15,27,28].

The characterization of the final system included the evaluation of the drug release in a vaginal fluid simulant to be more biorelevant followed by *in vitro* time-kill assay against *C. Albicans* again in a vaginal simulative medium.

As manufacturing devices, the possibility to create microfluidic systems using FDM has been explored. Microfluidics is an innovative, controllable, and scalable technique to produce nanocarriers. It relies on the precise control of micromixing in sub-millimeter channels driving to effective control of the final formulation characteristics by tuning the manufacturing parameters [9,29,30].

Compared to conventional bench techniques such as the thin layer evaporation method, microfluidics presents several advantages such as high reproducibility, low batch-to-batch variation, better control over particle characteristics, and easy scalability [31].

This technology also helps to overcome the main barrier in the translation of nanocarriers from the bench to the clinic that results in the scalability of the manufacturing technique.

Nevertheless, marketed microfluidic systems present some limitations comprising high cost, device fabrication expertise, and lack of versatility due to the fixed nature of the devices [8]. Thanks to 3DP it is possible to reduce complexity and costs and thus expand the realm of microfluidics [32] together with the possibility of personalization of the device. The FDM technique fits well this approach by the possibility of having a large selection of printing materials, low maintenance costs, ease of initial use, the ability to start, stop, and integrate complexity on the fly, and the possibility of full personalization of the device [33].

In the two works presented in this thesis, the first microfluidic device presented a T-shape and was printed using polylactic acid (PLA) (*Part II*) [8]. In this initial concept, the micromixing happens at the collision of jets reached through the energy input from the syringe pumps [34]. It represents an affordable microfluidic device with easy fabrication, low cost, and potential scalability even if, due to the nature of the polymer used, it is not compatible with aggressive solvents. Nevertheless, it possesses good compatibility with water and ethanol and since PLA is a biodegradable polymer, the chip could be disposed after some usage in the organic waste.

Using the developed 3DP microfluidic device, we formulated ethanolic liposomes by mixing soy phosphatidylcholine and cholesterol and carrying glycyrrhetinic acid to improve its poor solubility and bioavailability. This molecule is extracted from licorice and presents different activities such as anti-inflammatory, antioxidant, and others [35,36]. These nanocarriers were then physicochemically characterized and their cytocompatibility was assessed *in vitro*. Finally, their capacity to deliver the drug across skin mimicking membranes was evaluated and compared to the drug saturated solution.

Continuing this way, we thought to develop even more our idea of a 3DP microfluidic device coming to the optimized version presented in the third work (*Part III*) [9]. Compared to the PLA-based one, here, we used polypropylene (PP) as printing material since it is robust, flexible, and possesses wide compatibility with most organic solvents (*e.g.*, ethanol, methanol, acetone, acetonitrile) [37]. In this work, we developed two different devices with passive micromixing properties due to a zig-zag bas-relief in one and asymmetric circular subchannels in the other one. Thanks to the presence of these obstacles in the fluid streams, whirl flows and recirculation are created generating a transversal mass transport [38]. Even in this case, the 3D printed origin of the devices maintains all the advantages such as the possibility of personalization, low cost, easy set up, and potential scalability. The two developed 3DP microfluidic chips were tested by manufacturing a library of model liposomes and polymeric nanoparticles both encapsulating cannabidiol (CBD) as a model drug. Soy phosphatidylcholine and cholesterol were used as excipients for the liposomes meanwhile polymeric nanoparticles were prepared with polylactic-co-glycolic acid (PLGA). CBD was selected as a model drug thanks to its known properties comprising antioxidant, pain-relieving, and antineoplastic activities [39]. The formulated nanocarriers were firstly

characterized in terms of size, PDI, and encapsulation efficiency, and then a design of experiment (DoE) approach was applied to evaluate the influence of the manufacturing parameters in the final formulation characteristics.

Finally, in the last work (Part IV) [11], we have developed a 3D printed analytical device known as vertical diffusion cell (VDC) of Franz cell. This type of device is useful and routinely employed to evaluate both the release and permeation of active molecules from a donor formulation through a polymeric or biologic membrane [40]. Marketed VDCs are conventionally made of glass carrying the limitation of this material such as fragility and very careful handling. In this work, using PP due to its already mentioned characteristics, we 3D printed an alternative VDC to overcome the limitation of the glass-based ones with a lower overall cost of the analytical system. To confirm the applicability of our system, it has been compared with a commercially available glass system using a model caffeine solution with different membranes.

Part I

The content of part I has already been published in: Int. J. Pharm. (2021) 120290. https://doi.org/10.1016/j.ijpharm.2021.120290.

3D PRINTED CLOTRIMAZOLE INTRAVAGINAL RING FOR THE TREATMENT OF RECURRENT VAGINAL CANDIDIASIS

ABSTRACT

Vulvovaginal candidiasis is a vaginal infection caused by the fungal pathogen *Candida albicans* that, most commonly, affects women of reproductive age. Its first-line treatment consists in topical applications of conventional drug formulations (*e.g.*, creams, gels, tablets) containing imidazole drugs. The treatment involves single or multiple daily applications and, in the case of recurrences, daily administration of oral antifungal drugs for up to one month.

Intravaginal rings are flexible, biocompatible medical devices that, compared to conventional drug formulations, offer the possibility of a controlled vaginal drug delivery over a determined period with a single application, thus increasing patient compliance. Among innovative manufacturing techniques, in recent years, fused deposition modeling 3D printing has emerged in the pharmaceutical field to produce different therapeutics combining drugs and polymers. This technique allows to print objects layer by layer with many different thermoplastic materials after a computer-assisted design.

Thermoplastic polyurethanes are flexible and biocompatible materials that can be efficiently employed for the manufacturing of drug release systems, already utilized to prepare vaginal devices.

In this work, we produced a clotrimazole-loaded intravaginal ring by fused deposition modeling 3D printing combining the drug with thermoplastic polyurethane using hot melt extrusion. The rings were computer-designed and then printed with two different drug concentrations (*i.e.*, 2% and 10 % w/w).

The intravaginal rings were first tested in an agar-diffusion test to evaluate their effectiveness against *C. albicans*; and the 10% loaded ring was selected for further studies. Drug release was evaluated in two different media (*i.e.*, 50% ethanol and vaginal fluid simulant) showing a sustained release over a period of seven days. Next, *in vitro* time-kill analysis against *C. albicans* in simulated vaginal fluid was performed and displayed a complete growth inhibition after 5 days, compared to the control.

These results suggest a potential application of these 3D printed intravaginal rings for the treatment of vulvovaginal candidiasis and for the long-time treatment of recurrences.

Keywords: Topical application; vaginal device; additive manufacturing; controlled release.

1. INTRODUCTION

Vulvovaginal candidiasis (VVC) is among the most common vaginal infections in women of reproductive age caused by the opportunistic fungal pathogens *Candida albicans* and occasionally by other *Candida sp.* or yeasts [41]. These fungi are known to asymptomatically colonize many areas of the body of healthy individuals as part of the resident microbiota, including the gastrointestinal and genitourinary tracts. However, frequent antibiotic therapies, contraceptive use, alterations in host immunity, stress and other factors can lead to *C. albicans* overgrowth, causing a wide range of infections, from superficial mucosal to disseminated candidiasis, including VVC. Among the symptoms of VVC there are pruritus, vaginal soreness, dyspareunia, external dysuria, and abnormal vaginal discharge. During a lifetime, greater than 50 % of women aged 25 years and over, have suffered from VVC at some time, fewer than 5 % of these women experience recurrences. The optimal treatment for recurrent VVC has not yet been defined [25,42].

Among antifungal drugs, the class of imidazoles is still considered the first-line treatment for *C. albicans* infections. Clotrimazole (CTZ) is a synthetic derivative belonging to this class of molecules that possess a broad-spectrum antifungal activity against pathogenic dermatophytes and yeasts. It is present in the market in different pharmaceutical form (e.g., creams, tablets, ovules) and its mechanism of action rely on the inhibition of ergosterol synthesis and the alteration of the permeability of the cell wall [24]. The common treatment for VVC consists in single or multiple daily topical intravaginal applications of an imidazole cream from 3 to 7 days and, in the case of recurrences, the therapy should be continued with daily oral antifungal drugs up to 6 months, as first line maintenance regimen [25,42]. Despite CTZ is widely employed in the treatment of VVC, due to its poor solubility, repeated topical administrations are required to maintain a local therapeutic concentration.

Conventional vaginal medications (*i.e.,* solutions, emulsions, creams, etc.) are somewhat effective, but they still present several drawbacks such as i) leakage and messiness; ii) difficulty on providing an exact dose for creams and gels; iii) low retention to the vaginal epithelium; iv) poor patient compliance due to numerous repeated applications [43].

Compared to conventional vaginal dosage forms, intravaginal rings (IVRs) offer the possibility of a controlled vaginal drug delivery over a determined period with a single application [44]. IVRs are flexible devices made with biocompatible polymers with the advantages of safety, local application, few adverse effects, controlled drugs release and moreover, good patient compliance due to a one-time application for a long period of treatment [20]. The concept of sustained, localized drug administration to the human vagina using a polymeric ring was first published in 1970 [45] and since then, seven different rings have been marketed for hormone replacement or contraception [23]. Whereas for a long time IVRs have been developed only for hormonal therapy, in recent years there have been an increasing interest on this type of device as promising delivery system for microbicides against HIV, vaginal microbial infections and other sexually-transmitted diseases [28,44,46].

Among the manufacturing processes for IVRs production, an innovative and still not widely explored method is 3D printing [20]. Fused deposition modeling (FDM) is a 3D printing technique that allows to print objects layer by layer after a computer assisted design (CAD) using a wide range of materials.

In recent years this technique has emerged in the pharmaceutical field with multiple applications due to the possibility of combining drugs with different thermoplastic polymers using hot melt extrusion (HME) technique to produce the filaments needed to feed the printer [4].

Compared to conventional IVRs manufacturing techniques (e.g., extrusion or injection molding), with 3D printing, different shapes and dimensions can be easily produced to meet patients' needs and to increase acceptability and adherence [20,26].

Among materials that can be utilized with FDM, for the manufacture of IVRs, thermoplastic polyurethane (TPU) possesses the necessary characteristics of elasticity and flexibility, as well as a high potential to provide sustained drug release. Moreover, it has already been utilized to produce drug-loaded vaginal devices and marketed IVRs [15,27,28].

The aim of this work was to develop an innovative 3D printed IVR loaded with clotrimazole to treat vulvovaginal candidiasis providing higher patience compliance compared to the actual daily treatments. For this purpose, rings were printed using TPU previously loaded with two different concentrations of the antifungal drug CTZ using

the FDM technique. After an initial characterization, the drug release from the prepared IVRs was evaluated and then the *in vitro* antifungal activity was investigated against *C. albicans* to confirm the efficacy of the device over a period of 7 days.

2. MATERIALS AND METHODS

2.1 Materials

Thermoplastic polyurethane (TPU) Tecoflex^{TM} EG-100A was kindly gifted from Lubrizol (USA), clotrimazole (CTZ) was purchased from Fluorochem (UK). Sodium chloride, glacial acetic acid, sodium acetate, sodium lauryl sulfate (SLS), formic acid and pure ethanol were provided by Merck (Germany). DL-Lactic acid sodium salt 60% aqueous solution and lactic acid FU-BP were purchased from A.C.E.F. (Italy). All the other solvent used were HPLC grade.

2.2 Preparation of thermoplastic poly(urethane) (TPU) filaments containing clotrimazole (CTZ)

For the fabrication of 3D printed IVRs, FDM feeding filaments were prepared using HME by combining TPU and CTZ. An oil method was used to ensure an homogeneous distribution of CTZ on the pellets' surface, as previously reported [15]. Briefly, 30 g of TPU pellets were placed in a 50 mL conical centrifuge tube and 30 µL of castor oil were added. Next, the tube was vortexed for a few minutes to let the oil homogeneously cover all the pellets and then, the oiled pellets were transferred in a new 50 mL centrifuge tube to avoid wastage of drug that could remain stuck to the excess of oil still attached on the tube wall. At this point, a precise amount of CTZ, depending on the final concentration (2% and 10% w/w), was added and the tube was vortexed again to coat the pellets. The coated pellets were fed in the filament extruder (Noztek Pro HT, 3 mm nozzle, Noztek, UK) and extruded at 190 °C. To ensure homogeneity of the drug, the obtained filament was pelletized and extruded a second time using the same conditions to obtain the final filament with the diameter of 2.85 mm to be effectively printed. Blank IVRs were prepared using pure TPU filament produced by introducing TPU pellets (previously covered with castor oil) directly into the extruder at 190 °C. Composition of TPU filaments containing CTZ are reported in table 1.

Table 1. Composition of TPU filaments containing CTZ

Formulation	TPU (g)	Castor oil (µL)	CTZ (g)
TPU	30	30	0
2% CTZ	30	30	0.9
10% CTZ	30	30	3

2.3 Fabrication of 3D printed IVRs containing CTZ by FDM 3D printing

Drug-loaded and blank IVRs were printed with the previously prepared filaments using an Ultimaker 3 FDM 3D printer (Ultimaker, The Netherlands). The ring model with 54 mm of outer diameter (OD) and 4 mm of cross-sectional diameter (CSD) was designed with a CAD-based software and then converted to a print pattern using Ultimaker Cura 4.6 software (Ultimaker, The Netherlands). The layer height was set at 0.1 mm with 100% of infill density and a printing speed of 25 mm/s. The printing temperature was set at 220 °C with the build plate kept at room temperature.

2.4 Characterization of 3D printed IVRs

After 3D printing of the IVRs, they were weighed and the OD and CSD were measured using a digital caliper (Mitutoyo, Japan). Care was taken to ensure that the IVRs were not compressed or distorted during measurements. The elongation resistance was measured with a customized 3D printed system. TPU and CTZ before and after HME and 3D printing were also analyzed by attenuated total reflectance Fourier transformed infrared spectroscopy (ATR-FTIR, Spectrum Two FT-IR spectrometer with ATR accessory, Perkin Elmer, MA, USA). Measurements were performed at 450-4000 cm^{-1} with a resolution of 4 cm^{-1} and a total of 64 scans.

2.5 Microbial strain and culture conditions

The reference strain *C. albicans* ATCC 10231 was used in this study. The strain was routinely grown on Sabouraud dextrose agar (SDA) plates (VWR, Milan, Italy), incubated at 37 °C for 24 h. Stock cultures were maintained at -80 °C in nutrient broth (VWR) with 15% of glycerol.

2.6 Minimum Inhibitory Concentration (MIC) determination

MIC were determined by the standard micro-dilution method [47]. Firstly, a CTZ stock solution was prepared in DMSO of biological grade (2 mg/mL) and stored at 4 °C in the dark. Then, 100 µL of *C. albicans* ATCC 10231 suspension (10^6 CFU/mL), was diluted 1:50 in standard RPMI 1640 medium (Sigma-Aldrich, Milan, Italy) and inoculated into a 96-well plate together with the appropriate volumes of CTZ solution (0.0625-16 µg/mL). Two rows were left for control growth (inoculated medium without antifungal agent) and negative control (medium only), respectively. Preliminary assays with DMSO were carried out to exclude its possible antifungal activity; in any case, the volume of DMSO never exceeded 5 % (v/v). Plates were incubated at 37 °C and examined after 24 h. MIC is defined as the lowest drug concentration that inhibits the visible growth in comparison with the control. The turbidity of the 96-well plate was also measured using a spectrophotometer (530 nm) (Multiskan EX, Thermo Scientific).

2.7 Preliminary anticandidal assay in agar plates

At first, all the formulated IVRs (0, 2 and 10% CTZ) were sterilized by UV irradiation under flow safety cabinet for 1 h (30 minutes for each side) and maintained in sterile petri dishes. To perform the anticandidal assay, a modified agar diffusion method was used. Briefly, several colonies of *C. albicans* ATCC 10231 were inoculated into 15 mL of tryptic soy broth (TSB, VWR) and incubated at 37 °C for 24 h. At the end of the incubation period, the microbial suspension was adjusted to *ca* 10^6 CFU/mL (OD 600 nm 0.13–0.15), and 500 µL of this culture was added to 25 mL of liquid sterile SDA maintained at 50 °C; 15 mL were poured into a petri dish and allowed to solidify for several minutes, afterward the formulated IVR was placed on the solidified layer and the remaining 10 mL of inoculated SDA were poured to embed the medical device. This procedure was repeated for each formulated IVR in duplicate. The plates were then incubated at 37 °C for 24 h, and a well-defined zone of growth inhibition visible around each IVR was considered as index of antimicrobial activity.

2.8 *In vitro* clotrimazole release study

The *in vitro* release of CTZ from the 3D printed IVRs was evaluated in two different release media. The first was a 50% ethanolic solution and the second was a vaginal fluid

simulant (VFS) [48] added with 1% w/v of sodium lauryl sulfate (SLS). The addition of SLS was necessary to maintain sink condition due to the very poor solubility of CTZ in aqueous solvents [49].

For this study, the 3D printed IVRs were placed in sealed glass bottles with 100 mL of release medium to ensure that sink conditions were maintained. The bottles were then stored in an orbital shaking incubator at 37 °C, 100 rpm for seven consecutive days. During the first day, 1 mL samples were withdrawn every hour for the first 6 hours replacing the volume with fresh medium. Then, every 24 hours, a sample was withdrawn for the analysis and the total volume of release medium was replaced with fresh one. The amount of CTZ released from the IVRs was measured with a high performance liquid chromatography (HPLC) coupled with a diode array detector (DAD). The drug release from IVRs was evaluated in triplicate.

2.9 HPLC-DAD method for the analysis of CTZ

The amount of CTZ released during the *in vitro* studies was evaluated by HPLC (Agilent 1260 Infinity II, Agilent, USA) using a mixture of 0.5% formic acid in water and acetonitrile (ratio 55:45 for EtOH 50% release medium and 45:55 for VFS + 1% SLS release medium) as mobile phase, with a flow rate of 1 mL/min in an Agilent Zorbax Eclipse Plus C18, 150 x 4.6 mm, 5 µm column (Agilent, USA). The injection volume was 20 µL and the detection signal was recorded at 230 nm (UV lamp) keeping the analysis system at room temperature. Two different calibration curves of CTZ were performed with a concentration ranging from 0.005 to 0.2 mg/mL in EtOH 50% and in VFS + 1% SLS. The correlation coefficient (R^2) obtained was 0.9996 for both curves.

2.10 Time-kill assay

The time-kill studies curves allow to assess the exposure time required to kill a standardized *Candida* inoculum. In this study, vaginal simulative medium (VSM) [24] was used to simulate the typical environment of *Candida* infection in women. The composition of VSM was the following: bovine serum albumin (18 mg/L), NaCl (3.5 g/L), KOH (1.4 g/L), $Ca(OH)_2$ (0.22 g/L), lactic acid 90% (2.2 g/L), glycerol 50% (0.32 g/L), urea (0.4 g/L), glacial acid acetic (1 g/L), glucose (0.5% w/v) adjusted to pH 4.2. The medium was sterilized by 0.22 µm filter and maintained at 4 °C before use.

Two days prior the experiments, a series of sterile tubes containing 20 mL of VSM were prepared according to the following scheme: one tube with one 10% CTZ-IVR was incubated for 48 h at 37 °C (48h conditioned VSM 10% CTZ-IVR) with gentle shaking (100 rpm) and one tube with one 10% CTZ-IVR was incubated for 24 h at 37 °C (24h conditioned VSM 10% CTZ-IVR) with gentle shaking (100 rpm). The test organism *C. albicans* ATCC 10231 was incubated in 15 mL of TSB at 37 °C for 24 h. At the end of the incubation period, the microbial suspension was centrifuged at 3500 rpm for 10 min, the pellet was resuspended in the same volume of VSM and the turbidity was adjusted to *ca* 10^6 CFU/mL (OD 600 nm 0.15). 1 mL of this inoculum was added to the different sterile tubes containing 20 mL of VSM and the formulated IVRs, while in the unconditioned VSM sample, the 10% CTZ-IVR was added simultaneously with *C. albicans*. Lastly, one sterile tube containing 20 mL of VSM was inoculated as control growth together with one 0% CTZ-IVR. All the tubes were incubated at 37 °C with gentle shaking (100 rpm) and, at established time points (up to seven days: baseline, 24, 48, 72, 96, 120, 144 and 168 h), 100 µL aliquots were aseptically removed from each tube, serially diluted in sterile physiological saline solution and spread in triplicate (10 µL) onto SDA plates. After 24 h of incubation at 37 °C, the plates were observed and CFU were enumerated. All the experiments were performed three times using independent cultures.

3. RESULTS AND DISCUSSON

3.1 Fabrication and characterization of 3D printed IVRs

The materials utilized for the fabrication of IVRs require different mechanical characteristics such as elasticity and flexibility. The most common utilized ones are silicone elastomer, ethylene-vinyl acetate (EVA) and polyurethane [43,50]. In recent years, thermoplastic polyurethane (TPU) has shown great potential for the manufacturing of sustained release matrices and it has already been successfully employed in the development of vaginal devices and in 3D printing [15,51]. It is biocompatible and possesses the required physicochemical and drug release properties needed for the development of IVRs [23,28,52].

In this study, we intended to prepare IVRs for controlled release of CTZ using FDM 3D printing technology. In order to feed the printer, TPU pellets mixed with two different

concentrations of CTZ (*i.e.*, 2% and 10% w/w) were extruded via HME to produce smooth and flexible filaments with a diameter of 2.85 mm. The prepared filaments were clear, transparent with a light yellowish color increasing in intensity with the CTZ concentration.

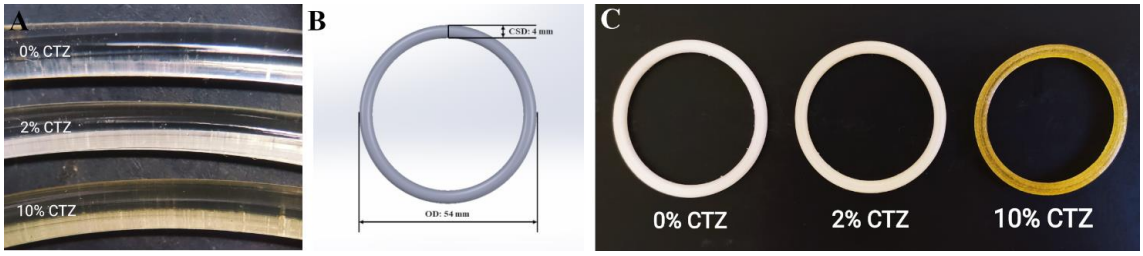

Figure 1. Fabrication of 3D printed IVRs: A) TPU filaments produced via HME loaded with different concentrations of CTZ; B) CAD 3D image of the IVR; C) 3D printed IVRs loaded with CTZ.

Using a stereo microscope (Nikon SMZ-1, Nikon, Japan), no visible aggregates of the drug were seen within the extruded materials (Figure 1A). An effective mixing was also due to the melting of CTZ during the extrusion process that ran at 190°C meanwhile the melting temperature of the drug is between 136.8 and 153.1 °C. The stability of the drug at the processing temperature is confirmed since it stays stable up to 340 °C when its thermal decomposition starts [53]. The thermal stability is a necessary condition for candidate drugs to be safely utilized in HME. Moreover, to reach a more homogeneous mixing, the filaments were cut again in pellets and extruded a second time. As previously reported [15], we confirmed again that it is possible to properly mix TPU and CTZ using a single screw extruder following the pellet coating oil method, avoiding the utilization of more advanced equipment such as a twin-screw extruder.

The prepared TPU filaments were used to feed the printer and prepare the IVRs by FDM technique. The ring was designed using a CAD software complying with the measures of commercial thermoplastic rings *i.e.,* an OD of 54 mm and a CSD of 4 mm (Figure 1B). Figure 1C shows the 3D printed IVRs produced with 0%, 2% and 10% of CTZ TPU filaments. The drug-loaded prototypes presented a yellowish color due to the presence of CTZ as already noticed during the production of the filaments. Immediately after printing, the rings were measured for their OD and CSD taking care not to compress or distort them during measurement and then weighted as reported in table 2.

All the manufactured rings were considered dimensionally accurate as they were within the specific acceptance criteria.

Table 2. Dimensional and mass analysis of produced IVRs

Sample	Mass (g)	CSD (mm)	OD (mm)
TPU-IVR	2.162±0.034	3.98±0.07	53.98±0.21
2% CTZ-IVR	2.175±0.021	4.05±0.05	54.03±0.17
10% CTZ-IVR	2.351±0.032	4.03±0.02	54.01±0.15

To establish whether any interaction had occurred between TPU and CTZ, the materials were analyzed by FTIR before and after HME, and then after 3D printing (Figure 2). FTIR spectra of raw materials presented the typical peaks [54,55] meanwhile any change in the peaks were noticed after the incorporation of the drug into the thermoplastic polymer suggesting that it was not affected by CTZ inclusion.

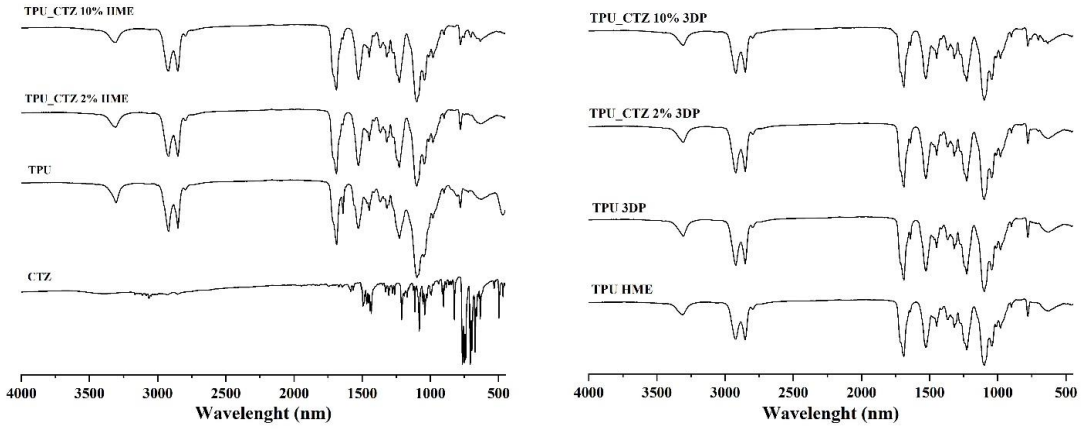

Figure 2. FTIR spectra of CTZ, TPU and their blends after hot melt extrusion (HME) and 3D printing (3DP).

Finally, to measure the elongation capacity of the 3DP IVRs, a customized 3D printed tensile testing jig with specifications reported elsewhere [56] was used. Tensile elongation is commonly used as a test method to assess the ultimate tensile strength of an IVR. It may reflect ring removal from the vagina, where a user hooks a finger around the inner diameter and pulls firmly to remove the device [56]. All the fabricated IVRs reached an acceptable elongation higher than 300% without breaking [28].

3.2 Antifungal preliminary studies

The results relative to the anticandidal activity of IVRs (CTZ 2 and 10%) and relative control (CTZ 0%) are presented in figure 3.

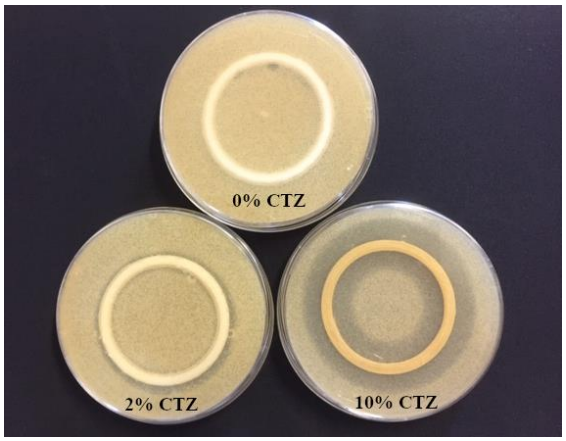

Figure 3. Preliminary antifungal activity of prepared IVRs, assessed by a modified agar-diffusion method.

The presence of the formulated IVRs resulted in a different inhibition of *C. albicans* ATCC 10231 growth. As shown in figure 3, in the plate with the highly CTZ loaded IVR (10% CTZ), the area of growth inhibition reached 2 cm (considering the IVR itself) compared to the negligible one observed for the IVR with 2% CTZ. The control TPU IVR without antifungal agent showed no growth inhibition. These preliminary studies suggested a possible effective antifungal activity of the 10% CTZ-IVR, that was then chosen for the following studies.

3.3 *In vitro* drug release studies

Whereas most of the currently marketed vaginal dosage forms are designed as immediate release formulations (*i.e.*, creams, gels, tablets, etc.), IVRs offer the possibility of a controlled vaginal drug delivery for a prolonged period of time with only one application. The IVR developed in this work is considered a matrix-type device in which the drug is homogeneously dispersed/dissolved in the matrix polymer and, drug release rates are proportional to both the drug loading and the surface area of the device [57]. A compendial dissolution method does not exist since monographs for IVRs are not present in the major international pharmacopoeia.

In this work, to evaluate drug release from IVRs, we utilized the shake-bottle method that was performed in an incubator shaker in which sealed bottles containing the IVRs and a specific volume of a pre-heated dissolution medium were placed. During this type of studies, it is essential to choose the appropriate dissolution medium for ensuring sink condition throughout the experiment. The use of vaginal fluid simulant media with physiological vaginal pH and osmolarity, represents a first setup towards physiologically relevant dissolution media for IVRs taking conditions as biorelevant as possible [44,50]. For this reason, VFS was chosen with the addition of 1% of SLS [58] to maintain sink conditions due to the poorly soluble drug used. Together with this medium, we also tested the drug release in a mixture of 50% ethanol in water [59] as solvent/water mixtures are recently become common for highly water-insoluble drugs [50]. Despite organic solvent mixtures are not as biologically relevant as media that simulate vaginal fluid, their utilization could be applied in quality control (QC) that normally requires discriminating and robust methods in which a biopredictivity is not required.

In figure 4, the cumulative and daily CTZ releases from the 3D printed 10% CTZ-IVRs are reported.

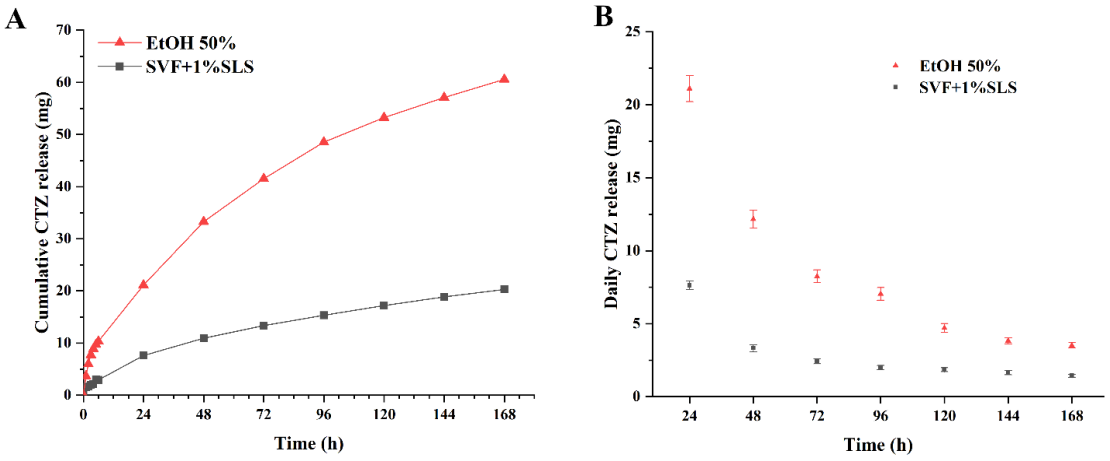

Figure 4. Drug release from 3D printed 10% CTZ-IVRs. (A) Cumulative CTZ release; (B) Daily CTZ release (mean ± SD, n=3)

The daily CTZ release ranged from 1.43 to 7.63 mg in the VFS and from 3.51 to 21.11 mg in the 50% EtOH medium showing a sustained release of the drug during seven days in both the tested media. The cumulative release resulted in 20.29 mg in VFS and 60.60 mg in 50% EtOH after one week. The amounts released were well above the MIC value

measured for *C. albicans* (0.0625 µg/mL) therefore, despite these results, the antifungal effectiveness was also tested *in vitro*.

In release studies, mathematical models play a crucial role in evaluating the drug release mechanism [60]. For matrix-type ring, like the one developed in this work, drug release under sink conditions normally adhere to the so-called "root-time kinetics". This is confirmed by a linear plot when the cumulative release data is plotted against the square root of time, a model first introduced by Higuchi in 1961 [61].

Here, the CTZ release data were fitted using the Higuchi equation giving a high linearity (R^2) of 0.998 in both the release media confirming the diffusion kinetic already reported in many other matrix-type IVRs [50,62–64].

3.4 *In vitro* effectiveness of CTZ-IVRs against *C. albicans*

The examined strain exhibited sensitivity to CTZ, showing MIC value of 0.0625 µg/mL. It was in accordance to those reported in the literature for *Candida* species isolated from vaginal infection [65].

Based on the antifungal preliminary data in agar, only the IVRs with 10% CTZ were used for the time-kill experiments in VSM. The antifungal effect of the formulated IVRs was confirmed on the tested *C. albicans* strain with an increased rate of microbial growth reduction during the entire incubation time (from 24 to 168 h) (Figure 5).

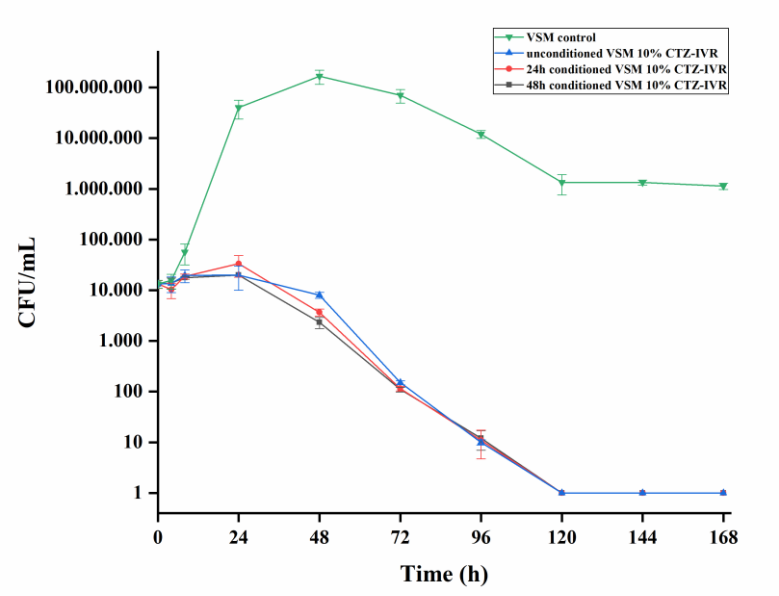

Figure 5. *C. albicans in vitro* time-kill experiment with 10% CTZ-IVRs pre-incubated for 24 and 48 h, incubated together with the fungi at time 0 and control incubated with 0% CTZ-IVRs.

In the performed experiments, the IVRs were left in VSM for 24 and 48 h to allow the release of CTZ in the medium prior to the addition of *C. albicans* ATCC 10231 suspension to simulate also a possible preventive antifungal application. As shown in figure 5, after 24 h of incubation, the viability of *C. albicans* decreased to $2x10^4$ CFU/mL in the 48h conditioned VSM CTZ-IVR and to *ca* $3x10^4$ CFU/mL in the 24h conditioned VSM CTZ-IVR, similar to the decrease ($2x10^4$ CFU/mL) observed in the unconditioned VSM CTZ-IVR. In all the IVRs-containing samples, after 24 hours the CFU/mL values were much lower compared to $4x10^7$ CFU/mL of the VSM growth control sample (with 0% CTZ-IVR) suggesting that the rings could be effective both in preventive or maintenance applications. The antifungal activity could be attributed only to the release of the drug since, in the VSM control containing the 0% CTZ TPU IVR, *Candida* growth was uncontrolled. In the following time points (from 48 to 96 h) a more drastic decrease of *C. albicans* viability was observed in all the CTZ-IVR samples (values ranging from $1.5x10^2$ to 10 CFU/mL), reaching the complete growth inhibition (no detectable CFU/mL) after 120 h of incubation.

From the analysis of the data, we can observe that the viability reduction caused by the formulated IVRs was not related to the conditioning of the VSM (for 24 and 48 h), probably because the daily CTZ released in the medium (Figure 4) resulted higher than CTZ MIC value. It can be noted that VSM presents features mimicking the physiological conditions during *C. albicans* growth in the vagina (low concentration of organic compounds, acid pH) [24], and this aspect is fundamental to have a better biopredictivity of the efficacy of the 3D printed IVRs.

4. CONCLUSIONS

For the first time, we have been able to produce 3D printed IVRs loaded with CTZ using FDM technique. The results obtained from *in vitro* studies against *C. albicans* are encouraging for possible applications against fungal infections. The drug release and time-killing studies were performed using media simulating the vaginal fluid to be more biorelevant.

As the common treatment for fungal infection consists in multiple applications of conventional dosage forms, the utilization of a vaginal device such the CTZ-loaded ring could improve the patience compliance by decreasing the number of applications to one

only switching from daily to weekly therapy. Moreover, the 3D printing technique allows the production of different shapes and sizes that can be helpful to have a personalized device based on the patient needs. Its utilization could be considered for immediate treatment perhaps together with conventional formulations and/or for maintenance therapy in case of recurrences instead of daily oral antifungal therapies.

Part II

The content of part II has already been published in: Int. J. Pharm. 584 (2020) 119436. https://doi.org/10.1016/j.ijpharm.2020.119436.

3D-PRINTED MICROFLUIDIC CHIP FOR THE PREPARATION OF GLYCYRRHETINIC ACID-LOADED ETHANOLIC LIPOSOMES

ABSTRACT

18-α-Glycyrrhetinic acid (GA) is an active molecule derived from licorice belonging to the family of triterpene saponin that exhibits many biological and pharmacological effects such as anti-inflammatory and antioxidant activities on the skin. However, the lipophilic nature and the very low solubility in water of GA, result in poor bioavailability that limits its clinical application. Different formulation strategies have been reported to overcome this barrier, including lipidic carriers such as liposomes. As drug delivery systems, liposomes present unique properties like biocompatibility, biodegradability, and the ability to carry both hydrophilic and lipophilic compounds and this has led to extended research in their use as topical delivery agents. Addition of permeation enhancers such as ethanol in these types of formulations helps the diffusion of these systems through the skin barrier. Hydrogelation of liposomes helps the topical delivery to the skin that remains the most preferred route due to the ease of administration, low cost, and patient compliance.

Microfluidics is an innovative and scalable technique interesting for the preparation of lipid-based nanovesicles that offers a precise control of micromixing under laminar flow. The necessary microchannel chip used with customizable characteristics could be 3D printed using a cost effective FDM printing technique.

Here, we aimed to formulate GA-loaded ethanolic liposomes, using a natural soybean lecithin, intended for local administration onto the skin. Using our 3D printed microfluidic chip, we prepared the vesicles that were firstly characterized for their physicochemical, thermal and morphological properties. Then, stability and drug encapsulation efficiency were measured, and, selected GA-loaded liposomes were evaluated for their cytocompatibility and skin permeation potentiality after hydrogelation using xanthan gum. The *in vitro* permeation studies were performed using Franz diffusion cells comparing two different media and three synthetic membranes including a polymeric skin-mimicking membrane.

As the formulation prepared presented no cytotoxicity and increased permeation compared to GA saturated hydrogel, it could perform therapeutically better effects than conventional formulations containing free GA, as prolonged and controlled release topical dosage form, which may lead to improved efficiency and better patient compliance.

Keywords: Drug Delivery; Fused Deposition Modeling (FDM); Hydrogel; Strat-M®; Vertical Diffusion Cell; Human Keratinocyte (HaCaT).

1. INTRODUCTION

Licorice (*Glycyrrhiza glabra L.*) is an herbaceous perennial legume native to warm countries, like Mediterranean countries and parts of Asia. The pharmacological properties of its root extract have been known since ancient times and it is used in many traditional Chinese medicines [66]. Its main bioactive compound, 18-α-Glycyrrhetinic acid (GA), a triterpene saponin that derives from the metabolism of glycyrrhizin, exhibits a remarkable broad spectrum of biological and pharmacological activities including antitumor [67], anti-inflammatory [35], antioxidant [36], antiviral [68], antimicrobial [69], antiulcer [70] and antidiabetic effect [71]. Particularly, licorice extrat demonstrated anti-inflammatory and anti-oxidant activities when applied topically onto the skin [72–74]. However, the lipophilic nature and the very low solubility in water of GA, result in poor bioavailability that limit its clinical application. In order to increase its absorption and thus its bioavailability, different formulation approaches have been reported and although enhanced GA concentrations led to an enhanced therapeutic effect it also led to enhanced side effects, such as hypertension [75]. To avoid possible side effect, topical delivery of GA could be an effective way to treat inflammatory skin diseases.

Topical delivery of drugs is a non-invasive route of administration that targets the skin and has limited systemic absorption thus minimizing the side effects. However, the presence of the stratum corneum hinders the delivery of the drug in the deeper layers of the skin in sufficient concentrations to exert its therapeutic effect [76]. Many formulation strategies have been reported in order to overcome this barrier, including carriers such as liposomes, niosomes and solid lipid nanoparticles [77]. Liposomes, as drug delivery systems, present unique properties like biocompatibility, biodegradability and the ability to carry both hydrophilic and lipophilic compounds and this has led to extended research in their use as topical delivery agents [78,79]. The presence of ethanol in high concentration into liposomal formulation leads to the formation of highly fluid vesicles (*i.e.*, ethosomes) allowing for penetration into deeper layers of the skin [80–83].

Another main issue regarding liposomal systems that inhibits their translation into the clinical environment, is their high production costs [84]. These high costs are mainly associated with the multiple steps needed during their preparation. The number of steps

is directly dependent on the preparation technique utilized. Among the different techniques reported for the production of liposomes, the ethanol injection method allows the direct preparation of small unilamellar vesicles (SUV) thus eliminating the step of size reduction necessary in most other techniques [85]. The ethanol injection method is simple, it avoids lipid degradation, and it is particularly suited for the preparation of ethosomes, as the ethanol in the final product doesn't have to be removed. Different strategies have been devised for the scaling up of this technique, including the membrane contractor method and microfluidic devices [30,86]. Many parameters such as the injection flow, the temperature as well as the stirring rate that affect the formation of the liposomal systems during their preparation with the ethanol injection technique, are difficult to control precisely. Microfluidics offers a precise control of micromixing under laminar flow and a highly efficient heat transfer and consequently presents an interesting alternative for the preparation of lipid-based nanovesicles [29,87].

In this work, authors developed ethanolic liposomal formulations loading 18-α-Glycyrrhetinic acid using microfluidics. A T-shape almost costless microfluidic chip 3D-printed with polylactic acid (PLA) using a fused deposition modeling (FDM) printer was used to obtain the final formulation. Prepared formulations were physicochemical characterized by average particle size, PDI and encapsulation efficiency. The best formulation with acceptable particle size, a narrow PDI and the highest encapsulation efficiency, was deeply investigated using Fourier transformed infrared spectroscopy (FTIR), transmission electron microscopy (TEM) and micro differential scanning calorimetry (mDSC). Subsequently, its cytocompatibility with human keratinocyte (HaCaT) was assessed. After hydrogelation of the formulation using xanthan gum, the permeation efficiency was tested *in vitro* using Franz diffusion cell compared to a GA saturated hydrogel. The liquid liposomal dispersion of the same formulation and a GA saturated solution were evaluated as well. Three different synthetic membranes (including a skin-mimicking one) and two different receptor media were utilized in order to evaluate differences in the permeation of the active compound.

2. MATERIALS AND METHODS

2.1 Materials

Polylactic acid 3D printing filament Innofil3D was kindly gifted from BASF (Germany), PVA printing filament was purchased from Ultimaker (The Netherlands), Phospholipon 90-G (P90G, soybean lecithin, 94 % of phosphatidylcholine) was kindly provided by Lipoid (Germany). 18-α-Glycyrrhetinic acid (GA) was provided by A.C.E.F. (Italy). 6-8 kDa and 12-14 kDa cut-off dialysis membranes (Spectra/Por® 7 and 4) were purchased from spectrum Lab (USA). Strat-M® membranes were purchased from Merck (Germany). Hydroxypropyl-beta-cyclodextrin (HPBCD) was provided by Roquette (France). All the other solvents used were HPLC grade.

2.2 3D-printing of PLA microfluidic chip

3D-printed PLA microfluidic chip was produced via fused deposition modeling (FDM) using an Ultimaker 3 printer (Ultimaker, The Netherlands)[88]. The T-shaped device was printed at a print speed of 30 mm/s and with a nozzle temperature of 215 °C. The infill density was set at 100 % and the build plate was preheated at 70 °C. The original 3D project was designed using SolidWorks 2018 software (Dassault Systèmes, France) and then converted to a print pattern using Ultimaker Cura 4.3 software (Ultimaker, The Netherlands). Alternating 50 μm thick layers were printed such that the pattern ran parallel to the length of the device, enabling leak-free and transparent devices to be printed with PLA. Supports for the model were printed using PVA, easily removed with warm water after printing. Through the printed T-shape microfluidic chip, the liquids were pumped in round shape capillaries with a diameter of 0.6 mm in order to reach a passive micromixing effect [34].

2.3 Preparation of ethanolic liposomes by microfluidic

For the preparation of liposomes by microfluidics, the 3D printed chip was connected to two syringes mounted on syringe pumps (AL1100, WPI Europe, Germany) through polyethylene tubing. The ethanolic solution containing P90G or P90G+GA was pumped against water at controlled flow rates and the samples collected from the end of the chip. The flows were controlled in order to reach a final amount of ethanol of 30 % v/v.

2.4 Preparation of ethanolic liposomes by ethanol injection method

Liposomes suspensions were prepared by a modified ethanolic injection method [85]. Briefly, the required amount of P90G was dissolved in ethanol and then, the resulting solution was injected with a controlled flow rate using a syringe pump (AL1100, WPI Europe, Germany) in a precise volume of distilled water under magnetic stirring at 600 rpm. The natural liposome formation occurred as soon as ethanolic solution was diluted into the aqueous phase. The liposome suspension was then kept under stirring for 5 minutes at room temperature.

For the preparation of GA loaded liposomes, precise amount of the active compound was dissolved into ethanolic phase together with P90G and, subsequently, injected into water under magnetic stirring using the same condition as for unloaded vesicles.

2.5 Liposomes physicochemical characterization

Prepared formulations were characterized for their average particle size (Z-average) and polydispersity index (PDI) by dynamic light scattering (DLS) using a Malvern Zetasizer Nano S instrument (Malvern Instruments Ltd, UK). The best formulation was also characterized by transmission electron microscopy (TEM, Philips CM10, 3 % uranyl acetate in 50 % ethanolic solution for negative staining) using an acceleration voltage of 80 kV to confirm its morphology and its size distribution. Briefly, for sample preparation, a droplet of liposomes suspension was deposed on a formvar-carbon-coated copper grid and then blotted using a filter paper. Subsequently a droplet of 3 % uranyl acetate in 50 % of ethanolic solution was added to the grid to obtain a negative staining. After removing the excess of liquid, the grid was washed with two droplets of water and air dried at room temperature. To further characterize the system, attenuated total reflectance Fourier transformed infrared spectroscopy (ATR-FTIR, Spectrum Two FT-IR spectrometer with ATR accessory, Perkin Elmer, MA, USA) studies were performed at 400-4000 cm^{-1} on freeze-dried liposomes pellets obtained after ultracentrifugation of the suspensions at 100000 G for 1 hour.

Heating scans were performed using a microDSC III instrument (Setaram, France) from 5 °C to 80 °C at a 1 °C /min rate after an isotherm at the initial temperature for 20 min for thermal equilibration. The mixture water/ethanol 70:30 v/v was used as reference. The transition temperature (°C) and enthalpy (J/g of solution) were calculated using the

tangent method (Setsoft2000 software, Setaram). Finally, the stability of liposomes was also evaluated by following changes on size and PDI of the nanoparticles after storage at 4 °C during 1, 14 and 30 days. Samples were withdrawn at each timepoint, and average particle size, PDI and encapsulation efficiency were measured. All the experiments were performed in triplicates.

2.6 HPLC method for the analyses of GA

The content of GA was assessed by high-performance liquid chromatography (HPLC Agilent 1260 Infinity II, Agilent, USA) using a mixture of 0.5 % formic acid in water and methanol (ratio 5:95) as mobile phase, with a flow rate of 1 mL/min in an Agilent Poroshell 120 EC-C18, 100x4.6 mm, 2.7 μm column (Agilent, USA). The injection volume was 20 μL and the detection signal was recorded at 276 nm (UV lamp) keeping the analysis system at room temperature.

2.7 Determination of encapsulation efficiency (EE%)

EE% was calculated by the percentage of drug encapsulated into liposomes (E_{drug}) relative to the total amount of drug added into the liposomal suspension (T_{drug}) using direct ultracentrifugation technique. Briefly, the liposomal suspensions were centrifuged at 100000 G for 1 hour. Following the pellets were dissolved in methanol in order to solubilize the vesicles and release the encapsulated drug entrapped. Then, the amount of GA was evaluated using HPLC as reported above. A calibration curve of GA standard was performed, with a concentration ranging from 0.01 to 0.1 mg/mL. A correlation coefficient (R^2) of 0.9985 was obtained.

The drug encapsulation efficiency (EE%) was calculated directly, as reported in equation (1):

$$EE\% = (E_{drug}/T_{drug}) \times 100 \qquad (1)$$

Where E_{drug} is the incapsulated amount measured with HPLC and T_{drug} is the total amount of drug used for the formulation.

2.8 Hydrogel formulations and chemico-physical characterizations

To prepare a topical applicable formulation, the selected best liposomal formulation was mixed with xanthan gum to form a hydrogel [89]. Briefly, 1 % w/v of xanthan gum was slowly added to vesicles suspension under stirring at room temperature. The formed hydrogel was left to stir as long as all the xanthan gum was solubilized and then stored at 4 °C before release studies. The rheological properties of the hydrogels were characterized using a rheometer (KinexusLab+, Malvern, UK) equipped with a cone-plate (C 40/4) geometry. A shear rate ramp test from 0.1 to 100 s^{-1} was performed for the determination of the viscosity (power law model) and an oscillation stress sweep test at 1Hz in the range of stress 0.1-50 Pa·s was performed for the determination of the linear viscoelastic region at 25 °C.

2.9 Cytocompatibility on human keratinocyte cell line (HaCat)

HaCaT cells (immortalized human keratinocytes) were grown in DMEM medium supplemented with 10 % fetal bovine serum, 2 % L-glutamine, and 1 % penicillin/streptomycin 100 U/mL, and maintained in a CO_2 incubator at 37 °C and 5 % CO_2. Cell culture reagents were from Merck (Milan, Italy). Cell viability upon administration of unloaded (F7 formulation) and loaded liposomes (F8 formulation) to HaCaT cells was analyzed by WST-8 and sulphorodamine B (SRB) assays, which evaluate cell metabolic activity and cell protein content, respectively. Briefly, cells ($5x10^3$/well) were seeded in 96-well plates and treated for 24 h with unloaded or loaded liposomes at different concentrations (from 25 to 250 µg/mL). After incubation, WST-8 (Merck, Milan, Italy) was added to each well, and cells further incubated at 37 °C up to 4 h [90]. Color development was monitored at 450 nm in a microplate reader (BioRad Laboratories, Hercules, USA). In the same 96-well plate, SRB test was then performed, as previously published [91]. Briefly, cell culture medium was removed, cells fixed with 50 % trichloroacetic acid and incubated with 0.4 % SRB solution (Merck, Milan, Italy). After rinsing with 1 % acetic acid and solubilizing in 10 mM Tris, absorbance was measured at 570 nm. Data were expressed as cell growth (%) versus non-treated cells (controls).

2.10 *In vitro* permeation test evaluation using different membranes and receptor media

In vitro diffusion studies were carried out using Vertical Diffusion Cells (VDC or Franz diffusion cells, Teledyne Hanson Research, USA) with a receptor compartment volume of 7 mL and an effective diffusion area of 1.766 cm^2. Two different receptor media were used to fill the receptor chambers and evaluate the influence in drug permeation: i) 30 % (v/v) ethanolic phosphate buffer saline (PBS) pH 7.4 and ii) 0.5 % (m/V) of HPBCD in PBS pH 7.4 [92]. The receptor media in receptor chambers were continuously stirred at 600 rpm with magnetic bars coupled with helixes. The system was thermostated at 32 ± 5 °C with a circulating jacket. Three different membranes were tested in order to evaluate and compare differences in diffusion: i) MWCO 6-8 kDa dialysis membrane (Spectra/Por 7 Standard RC Dry Dialysis Tubing Spectrum Labs, USA); ii) MWCO 12-14 kDa dialysis membrane (Spectra/Por 4 Standard RC Dry Dialysis Tubing Spectrum Labs, USA); iii) Skin-mimicking Strat-M® membranes which comprise two layers of polyethersulfone on top of one layer of polyolefine. These polymeric layers create a porous structure with a gradient across the membrane in term of pore size and diffusivity. The porous structure is impregnated with a proprietary blend of synthetic lipids, imparting additional skin-like properties to the synthetic membrane [93]. At predetermined sampling intervals (1, 2, 4, 8, 12 and 24 h), samples were withdrawn from the receptor compartment and replaced with an equal volume (0.2 mL) of fresh buffer. The content of the active compound in each sample was then determined by HPLC as reported above.

The amounts of the active compound released at each time point (AR_{tn}) were obtained using the eq. (2) for the first time point and eq. (3) for the subsequent time points:

$$AR_{t_1} = \frac{C_{t_1} * 1000 * V_c}{A_o} \qquad (2)$$

$$AR_{t_n} = \frac{C_{t_n} * 1000 * V_c}{A_o} + (AR_{t_{n-1}} * \frac{V_s}{V_c}) \qquad (3)$$

where AR (μg/cm^2) is the amount released at t_n sampling interval, the C_t (mg/mL) is the concentration of GA (mg/mL) determined at t_n sampling interval, V_c (mL) is the volume of diffusion cell receptor compartment, A_0 (cm^2) is the diffusion surface area of sample well and V_s (0.2 mL) is the sampling aliquot volume. Liposomal formulation ethanolic hydrogel (30 % of ethanol) and 30 % ethanolic saturated GA hydrogel and their corresponding suspension and solution were tested using this system.

2.11 Statistics

The data presented are the mean ± standard deviation of triplicate measurements and are representative of at least three independent experiments

3. RESULTS AND DISCUSSON

3.1 Characterization of formulated liposomal suspensions

Two different methods were used to prepare plain and GA loaded liposomes. The common ethanol injection method (EI) was contrasted to a microfluidic approach (MF) and the quality of final formulations was evaluated. Compared to common formulation techniques, microfluidics shows significant advantages, such as a smaller particle size distribution, higher reproducibility, improved EE% and enhanced scaling-up potential [94]. This is due to the unique behavior of fluids on the micro-scale where surface and viscous forces dominate over gravity and inertia, giving rise to laminar flow in single phase systems, and reproducible and programmable droplet flow in multiphase systems [95]. Despite these unique properties, microfluidics has largely remained a specialist research area not accessible to everyone due to specific manufacturing methods with high costs (for example lithography) and versatility due to the fixed nature of the fabricated devices. Nowadays, the most prevalent and accessible 3D printing technology is fused deposition modeling (FDM) that with recent advances has gained the resolution necessary to fabricate in the microscale without sophisticated manufacturing centers [10,88]. Our self-fabricated 3D printed PLA microfluidic chip represent an affordable microfluidic device with easy on fabrication, very low cost and potential scalability for

higher production rates. Furthermore, besides PLA is not compatible with aggressive solvent such as acetone it possess a good compatibility after printing for water and ethanol [96] and it is considered a biocompatible and biodegradable polymer [97] that can be easily disposed after some usage.

Taking advantages of this manufacturing process, the microfluidic chip was designed with a T-shape configuration in order to have a passive micromixing at the collision of jets reached through the energy input from pumping power [34].

Different amounts of P90G were used to prepare plain liposomes and GA loaded liposomes with the two techniques, as reported in Table 1. Ethanol used to dissolve P90G and GA was left into the final formulations (30 % v/v) to act as skin permeation enhancer [98,99]. The amount of GA used (0.5 mg/mL) was selected after testing different GA concentrations as the highest without any precipitation of the active compound in the final formulation (data not shown). Moreover, different flow ratios were tested as this parameter affects the final physicochemical characteristics such as size and PDI and the best one was chosen to produce all the formulations reported in table 1.

Table 1. Characterization of prepared liposomal formulations

Sample	**Technique**	**P90G (mg/mL)**	**GA (mg/mL)**	**Average size (nm)**	**PDI**	**EE%**
F1	EI [a]	10	0	122±2	0.167±0.03	0
F2	EI	10	0.5	196±6.1	0.275±0.05	26.4±4.1
F3	EI	20	0	178±1.6	0.213±0.01	0
F4	EI	20	0.5	271±2.4	0.374±0.04	50.14±3.1
F5	MF [b]	10	0	100±1.8	0.200±0.001	0
F6	MF	10	0.5	110±2.6	0.233±0.03	37.32±3.2
F7	MF	20	0	169±1.5	0.202±0.07	0
F8	MF	20	0.5	202±5.2	0.260±0.01	63.15±2.2

[a]Ethanol injection technique (EI); [b]Microfluidic technique (MF).

Afterwards, blank and loaded liposomes were characterized by measuring their average size, PDI and encapsulation efficiency (Table 1). On average, taking advantages from the potentiality of microfluidics, formulations prepared with this technique presented an

average size with narrow distribution, acceptable PDI and increased EE%. For all the formulations prepared, increasing the amount of lipids led to an increased encapsulation efficiency and a slight increase on the average hydrodynamic diameter. All the microfluidics-prepared formulations presented better physicochemical characteristics compared to ethanol injection method thanks to the fabricated, low-cost microfluidic chip. According to these preliminary results, formulation F8 was selected for further investigations. This formulation presented an average size of 202±5.2 nm, a moderate polydispersity index and an encapsulation efficiency of 63.15 %, the highest reached for the developed formulations. All these characteristics were better than the formulation obtained by ethanol injection using the same amounts of lipids and GA.

The size distribution and morphology of selected formulation were also studied by TEM (Figure 1). Despite vesicles exhibited a similar average size according to DLS measurements, some differences between the two techniques were noticed, confirming the moderate dispersity of the prepared liposomes. This phenomenon has been already reported in the literature and it is due to the measurement characteristics of DLS that highlights the larger particles in the whole sample. Contrarily, when observing the sample by TEM, it is possible to visualize also smaller vesicles that are underestimated by DLS [100]. Regarding morphology, the majority of the vesicles showed a symmetric and spherical shape.

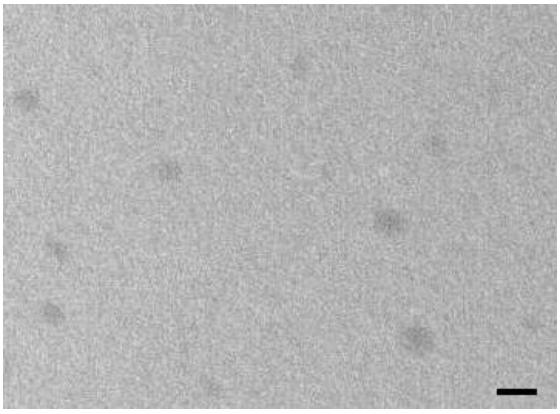

Figure 1. TEM (Transmission electron microscopy) images of F8 formulation. Scale bar 400 nm

Additionally, FTIR spectroscopy analysis was performed on freeze-dried F7 and F8 formulation pellets obtained after ultracentrifugation to evaluate the difference between unloaded and loaded vesicles (Figure 2). For GA, the peak at 3450 cm^{-1} was attributed

to the absorption of O-H stretching vibration meanwhile, stretching vibrations of C-H groups appeared in the range of 2850-2970 cm^{-1} and the C=O vibration emerged at 1730 cm^{-1} [101]. The peak at 1650 cm^{-1} was attributed to the C=O of C=C-C=O [102]. This peak appeared increased in the loaded formulation suggesting the presence of GA.

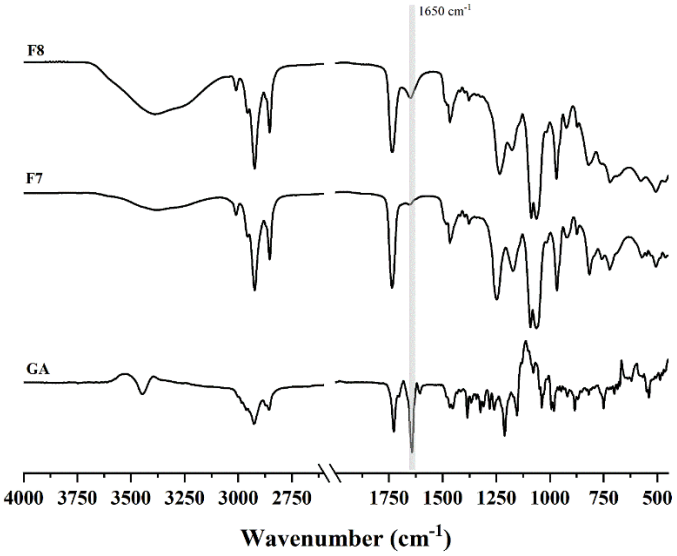

Figure 2. Fourier transformed infrared spectroscopy (FTIR) of 18-α-Glycyrrhetinic acid (GA), plain liposomes (F7) and GA loaded liposomes (F8)

The chemical-physical differences between unloaded and loaded vesicles were further investigated by micro differential scanning calorimetry (mDSC). The obtained thermograms showed the typical profiles of liposomal dispersions formed by a phospholipid mixture [103]. Indeed, a broad endothermic transition was recorded between 5 °C and 70 °C, resulted from the sum of the contribution of the of phospholipids composed of fatty acids with a different length. The effect exerted by the encapsulation of GA into P90G-based liposomes is not marked. However, in loaded liposomes a slightly lower transition temperature (30.75±1.56 °C and 36.96±1.27 for formulation F8 and F7, respectively) and a slightly lower enthalpy associated to the transition (0.877±0.048 J/g of solution and 1.102±0.131 J/g of solution for formulation F8 and F7, respectively) suggest a possible interaction between GA and the phospholipid bilayer. P90G, exhibits an intrinsic thermotropic behavior, which is independent on the presence of the solvent, as revealed by the similar endothermic transitions in the range 10-70 °C of the materials at the solid state (Supplementary

Figure). Besides, other common lipid materials used for the formulation of vesicles (e.g. monooleins or phytantriol) show different thermal transitions at the solid state and as aqueous dispersions [104,105]. More details can be found in the supplementary materials.

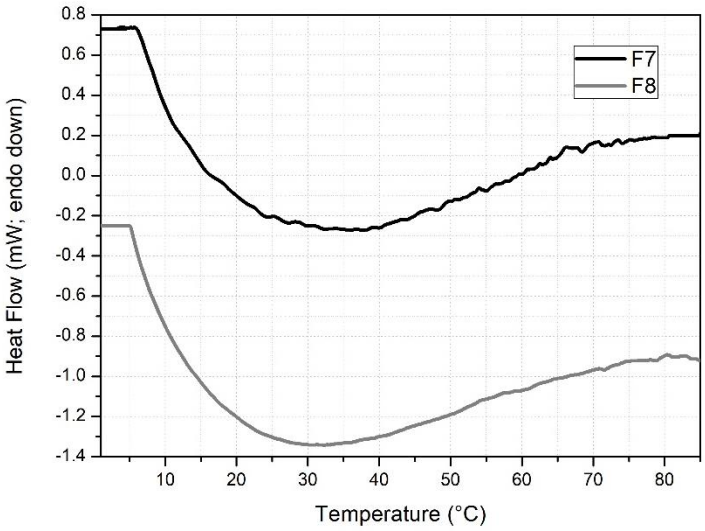

Figure 3. Micro differential scanning calorimetry (mDSC) heating traces for plain liposomes (F7) and GA-loaded liposomes (F8).

3.2 Stability studies

The stability of the selected formulation (F8) was assessed by following changes in average size, PDI and EE% after 1, 14 and 30 days of storage at 4 °C (Table 2). Over one month of storage period, the average vesicle size was found in the range of 205-232 nm and the PDI in the range of 0.258-0.274. The encapsulation efficiency decreased during one month from 62.8 % to 58.5 %. Drug leakage from vesicles during a storage period was noticed also in other studies and most probably it is due to the low rigidity of the bilayer that promotes drug leakage [106–108].

Table 2. Stability studies (average size, PDI and EE%) of formulation F8 during 1, 14 and 30 days at 4 °C.

TIME (Days)	**AVERAGE SIZE (nm)**	**PDI**	**EE%**
1	205±1.4	0.258±0.01	62.8±1.9
14	225±4.1	0.265±0.03	60.5±2.7

30	232±2.6	0.274±0.03	58.5±1.5

3.3 Hydrogel formulation and rheological studies

As the formulation prepared was intended for skin topical application, the liposomal dispersion F8 was formulated into a hydrogel using 1 % w/v xanthan gum. Xanthan gum is a polysaccharide composed of pentasaccharide repeating units of glucose, mannose and glucuronic acid in a 2:2:1 molar ratio suitable for biomedical application and already used as supporting hydrogels for drug release applications [89].

Studies were performed to evaluate the influence of blank (F7) and GA liposomes (F8) on the hydrogel viscosity and rheological behavior. The presence of vesicles did not affect the viscosity of the 1 % w/v xanthan gum hydrogels. Indeed, a viscosity of 14.20±1.49 Pa·s was determined for the hydrogels without vesicles (dispersion medium water/ethanol 70:30), while a viscosity of 13.68±1.02 Pa·s and 13.4± 0.98 Pa·s was determined for hydrogel prepared in presence of blank or GA-loaded vesicles, respectively (Supplementary figure). The viscoelastic properties also were not affected at least in term of the limit of the linear viscoelastic region (LVR), which was ~10 Pa·s for all analyzed systems (Supplementary figure).

3.4 Cytocompatibility on human keratinocyte cell line (HaCaT)

The cytotoxic effect of nanoparticles, which mainly relies on non-specific and specific cell-nanoparticles interactions, is affected by different intrinsic properties of the nanomaterials such as size, shape, composition and surface charge [109,110]. In order to study the *in vitro* cytocompatibility of the prepared vesicles, different concentrations of blank (F7 formulation) and GA liposomes (F8 formulation) up to 250 µg/mL were incubated for 24 h with HaCaT keratinocytes, a transformed epidermal human cell line [111] (Figure 4).

All the tested concentrations of vesicles for both loaded and blank liposomes exhibited no cytotoxicity after 24 h of incubation with more than 95 % of cell viability, equally in the two assays used.

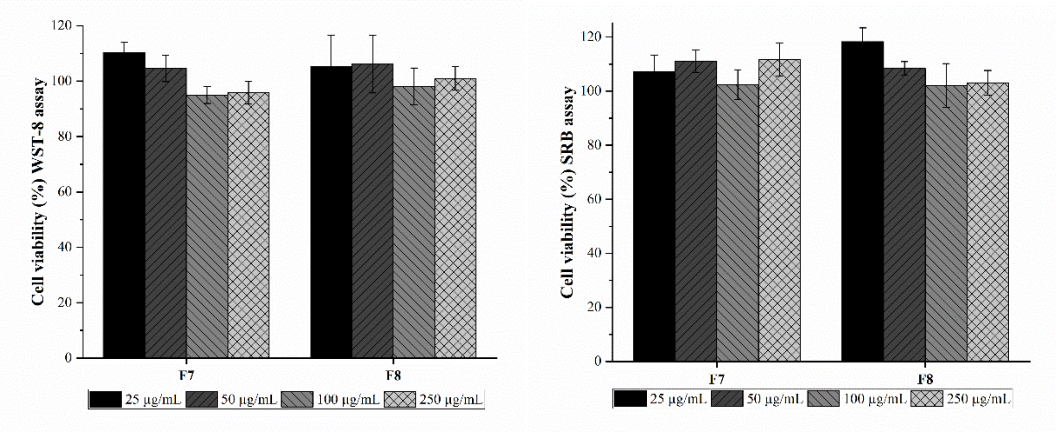

Figure 4. Cell viability of HaCaT cell line after incubation with unloaded liposome (F7) and GA loaded liposomes (F8) at different concentrations for 24 h at 37 °C. The viability was determined by WST-8 and SRB assays and all data sets were compared with the control (unloaded liposomes). Error bars represent the mean ± SD.

3.5 *In vitro* permeation test evaluation using different membranes and receptor media

In vitro permeation experiments using excised human and animal skins can be effective to study the skin permeation profiles of topically applied active compounds. However, they are expensive and possess several drawbacks that hinder reproducibility data such as variations of skin thickness, diseased skin states, preparation complexity, age of donor, density of hair follicles and skin storage conditions [112]. In this study we used synthetic Strat-M® membranes that possess human skin-like properties as a reproducible alternative to excised human skin [112]. Moreover, together with Strat-M® membranes, we compared two cellulose dialysis membranes with different cut-offs (i.e. 6-8 kDa and 12-14 kDa) that are usually employed in studies with vertical diffusion cells [113–115]. Together with these different membranes, we studied the influence of receptor media during the studies with Franz diffusion cells using EtOH 30 % and HPBCD 0.5 % as model solution with enhanced solubility for GA [92].

Release study results showed an enhanced permeability through all the three type of membrane tested for the liposomal hydrogel formulation F8 compared to the GA saturated hydrogel. This behavior is due to an increased GA solubility after its interaction with phospholipids. The best receptor medium suitable for our studies was 30 % ethanolic solution in PBS pH 7.4 where the active compound resulted more

soluble reaching a maximum amount released 86±3 µg/cm^2 compared to the maximum reached using HPBCD 0.5 % in PBS pH 7.4 that was only 23.6±2.4 µg/cm^2 after 24 hours.

As expected, liposomal suspension reached a higher release compared to liposomal hydrogel that possesses an increased controlled and sustained release behavior [89]. Between different membranes, after 24 hours, the highest permeation happened through cellulose membrane with 12-14 kDa cut-off (80.5±5.8 µg/cm^2) followed by 6-8 kDa cut-off (71.6±5 µg/cm^2) to finish with Strat-M® membrane (62.4±3.5 µg/cm^2). This is due to the higher permeability of cellulose membrane compared to Strat-M® that is formed by three different layers and impregnated with a blend of synthetic lipid to mimic in the best way possible human skin.

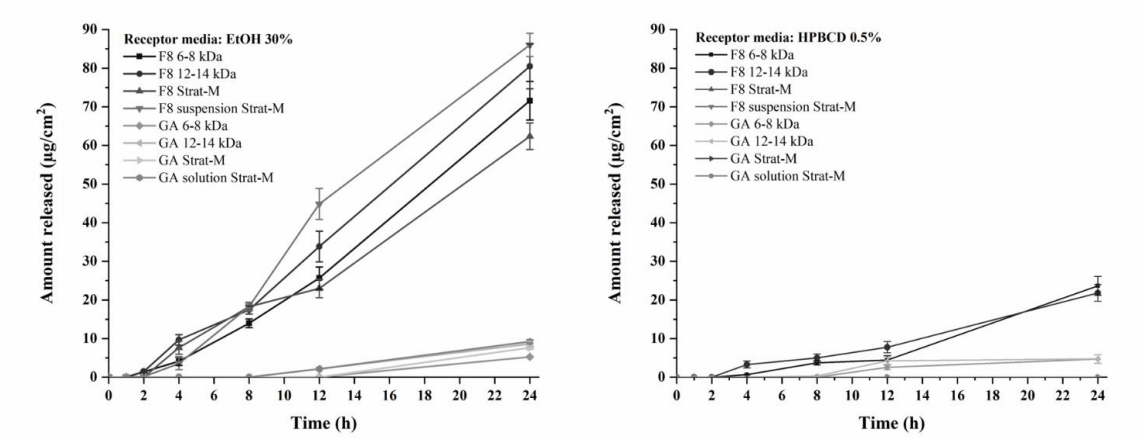

Figure 5. *In vitro* release studies using vertical diffusion cells with two different receptor medias: Ethanol 30 % in PBS pH 7.4 and Hydroxypropyl-beta-cyclodextrin 0.5 % w/v in PBS pH 7.4. In the two graphs, the liposomal hydrogel from F8, the liposomal suspension F8, saturated GA hydrogel and saturated GA solution are represented.

4. CONCLUSIONS

In this work, we have formulated an ethanolic liposomal formulation encapsulating GA as active compound and using natural soybean lecithin, intended for topical administration. To produce liposomal dispersions with good physicochemical characteristics and an EE% of GA up to 63 %, we used a biodegradable and cost-effective PLA 3D-printed microfluidic chip which represents an affordable microfluidic device with an easy fabrication, very low cost (13 g of PLA for a total cost of less than

1 US $) and potential scalability for higher production rates. In particular, with one of our 3D printed chips it is possible to produce up to 900 mL/h of formulation and for higher production, more than one chip can be run in parallel at the same time.

The effect of different receptor media and membranes on the release of GA from the xanthan gum-based hydrogels prepared from the liposomal dispersions was assessed using Franz diffusion cell apparatus. In our studies we noticed that the selection of the membrane is a fundamental step because generic membranes such as regenerated cellulose can provide evidence on important changes associated with the size of the drug evaluated and the vehicle used to dissolve it as already reported in another study [114]. The use of standardized Strat-M® membranes could represent a reproducible methodology as substitution of ex-vivo skin in diffusion studies using VDC [93,112].

Differences have also been noticed between the two analyzed receptor media (ethanol 30 % v/v or HPBCD 0.5 % w/v in PBS pH 7.4) and, as already reported in literature, the observed different release is related to the solubility of the active compound in specific solutions. According to this, the best receptor medium, for our purposes, resulted 30 % ethanolic solution in PBS allowing a much higher amount of drug released. Overall, we demonstrated that GA loaded in liposomal vesicles, both as liquid dispersions and incorporated into a hydrogel formulation can permeate almost 10x time than its saturated solution.

The proposed formulation can be easily scalable thanks to the microfluidic technology and utilized for preparing hydrogels for topical application, showing an efficient release of GA, and possibly for other hydrophobic active compounds.

Part III

The content of part III has already been published in: Int. J. Pharm. 599 (2021) 120464. https://doi.org/10.1016/j.ijpharm.2021.120464.

MICROFLUIDICS FOR NANOMEDICINES MANUFACTURING: AN AFFORDABLE AND LOW-COST 3D PRINTING APPROACH

ABSTRACT

During the last decade, an innovative lab on a chip technology known as microfluidics became popular in the pharmaceutical field to produce nanomedicines in a scalable way. Nevertheless, the predominant barriers for new microfluidics users are access to expensive equipment and device fabrication expertise.

3D printing technology promises to be an enabling new field that helps to overcome these drawbacks expanding the realm of microfluidics. Among 3D printing techniques, fused deposition modeling allows the production of devices with relatively inexpensive materials and printers reducing the resources and skills required to manufacture microfluidic devices.

In this work, we developed two different microfluidic chips designed to obtain a passive micromixing by a "zigzag" bas-relief and by the presence of "split and recombine" channels. The two designs were evaluated with computational fluid dynamic studies showing an effective mixing potential. The microfluidic chips were printed with a fused deposition modeling 3D printer using polypropylene as manufacturing material. With them, we formulated two different model nanocarriers (*i.e.*, polymeric nanoparticles and liposomes) evaluating the influence of manufacturing parameters with a design of experiments applying a 2-level full factorial design. Next, we encapsulated cannabidiol as a model drug measuring the encapsulation efficiency.

Both the chip showed an effective production of nanocarriers with controllable characteristics and with a good loading degree.

These polypropylene-based microfluidic chips could represent an affordable and low-cost alternative to common microfluidic devices for the effective manufacturing of nanomedicine (both polymer- and lipid-based) after appropriate tuning of manufacturing parameters.

Keywords: FDM; nanomedicine; polymeric NPs; liposomes; cannabidiol; drug delivery systems, CFD.

1. INTRODUCTION

The scale up of nanocarriers production is one of the main issues for the translation from the bench to the clinic of innovative drug delivery nanosystems (DDS) [116]. Common methods such as thin layer evaporation or nanoprecipitation involve several steps and usually lack of reproducibility, controllability, and low production rate [117]. In a typical colloidal system production, the procedure is based on a bottom-up approach, where most of the theoretical works describing the formation process are based on the classical nucleation theory [94,118].

To better control the manufacturing parameters and the final formulation characteristics, during the last few years, the concept of lab on a chip became popular among researchers facilitating the development of more precise systems for healthcare applications by the miniaturization of conventional processes [119,120]. Among different lab on a chip technologies, microfluidics became an innovative manufacturing approach in the pharmaceutical and biomedical fields by manipulating nanoliters scale of fluids in submillimeter channels [30].

Even if the microfluidic method is not a new story, the colloidal DDS-assisted production has drawn increased interest due to several advantages such as high reproducibility, low batch-to-batch variation, better control over particle characteristics, and ease to scale-up [31]. Moreover, microfluidics can sharply increase the surface area-to-volume ratio by several orders of magnitude allowing a more efficient mass and heat transfer within the system [121].

The production of nanocarriers within this technique needs mixing of fluids in sub-millimeter channels that become difficult into simple smooth microchannels in which the flow remains laminar. To overcome this problem different micromixers have been developed and classified as active and passive micromixers [34]. Active micromixers take advantage of external sources of energy such as electric or magnetic fields and acoustic waves. Even if the mixing is rapid within these devices, they are more difficult to fabricate, integrate, and operate compared to passive micromixers. Passive micromixers are based on shape modification of the microchannels to produce a specific flow pattern that enhances mixing such as the presence of obstacle, bas-reliefs, or split and recombine microchannels that induce whirl flow and recirculation creating transversal mass transport [38].

Common microfluidic device fabrication protocols include photolithography and micromachining. The predominant barriers for new users and alternative applications are access to expensive equipment and device fabrication expertise.

3D printing technology promises to be an enabling new field that reduces complexity and costs and thus expands the realm of microfluidics [32]. Among the 3D printing techniques currently available, fused deposition modeling (FDM) utilizes a heated nozzle to extrude a thermoplastic polymeric filament layer over layer to form the desired 3D object [4]. This approach presents several advantages including relatively inexpensive materials and printers, low maintenance costs, a large selection of commercially available materials, the ease of initial use and the ability to start, stop, and integrate complexity on the fly [33].

Compared to expensive microfluidic chip production techniques, 3D printing enables a reduction in the resources and skills required to manufacture microfluidic devices, micromixer included as already reported in the literature [10,122–124].

In this work, we developed two different 3D printed microfluidic chips using polypropylene (PP) in an FDM 3D printer. The two chips rely on passive micromixing due to the presence of a "zigzag bas-relief" and a "split and recombine" channel shape, respectively. PP was selected as the manufacturing material because it is a robust, flexible, and chemically inert polymer, resistant to the majority of organic solvents such as acetone, acetonitrile, ethanol, and methanol. [37].

The microfluidic designs were first characterized by computational fluid dynamics (CFD) studies and then printed to be evaluated for the manufacturing of nanocarriers.

Both lipid-based and polymer-based nanocarriers were produced and characterized, encapsulating cannabidiol (CBD) as a model active molecule since it has shown different therapeutic effects such as anti-inflammatory, pain-relieving, antioxidant, immunomodulatory, antidepressant, antiepileptic, anticonvulsant and, antineoplastic effects [39]. The influence of manufacturing parameters was evaluated with a design of experiment (DoE) approach.

2. MATERIALS AND METHODS

2.1 Materials

Neutral polypropylene 3D printing filament was kindly gifted from Verbatim (Italy), Phospholipon 90-G (SPC, soybean lecithin, 94 % of phosphatidylcholine) was kindly provided by Lipoid (Germany), cholesterol was kindly provided by Croda (United Kingdom), poly(lactic-co-glycolic acid) (PLGA Purasorb® 5002A) was kindly provided by Corbion (The Netherlands). Cannabidiol (CBD) was purchased from VerusHemp (United Kingdom). All the other solvents used were HPLC grade.

2.2 Design of microfluidic chips

The original 3D projects were designed using the computer aided design (CAD) software SolidWorks 2018 (Dassault Systèmes, France). The two designs were developed to have an effective passive micromixing with "zigzag" bas-relief and "split and recombine" channels. The files were exported from the CAD software as STL (Stereolithography interface format) to be then converted in machine language with a computer aided manufacturing (CAM) software (STL file provided as supplementary material).

2.3 Computational fluid dynamics studies

The single-field incompressible Navier–Stokes equations modeled with the volume-of-fluid (VOF) method was used for the CFD simulations of two-phase flow [125]. The VOF model is a surface-tracking technique that uses a fixed mesh system to solve geometry interfaces and interactions between different fluids. The fluid dynamics of two-phase flows are described with a set of single-field equations which are obtained through conditional volume averaging of the local instantaneous conservation equations of mass and momentum.

The indicator function (α) allows obtaining the location of the interface, which is equal to the volume fraction of a phase in each cell. The solution of the continuity equation (1) for the volume fraction (α) of one of the phases enables to track the evolution of the interphase surface [125].

$$\frac{\partial \alpha}{\partial t} + \nabla \cdot (\alpha U) = 0 \qquad (1)$$

where α is the volume fraction and U is the velocity field. Since α is discontinuous at the phase boundaries, and it is important to have this discontinuity sharp enough to precisely capture the interface between two phases, an additional term has been introduced, which is a function of the relative velocity between two phases U_r, as in equation (2).

$$\frac{\partial \alpha}{\partial t} + \nabla \cdot (\alpha U) + \nabla \cdot (\alpha(1-\alpha)U_r) = 0 \quad (2)$$

It is worth noticing that the equation is exact because no assumptions are employed in its derivation.

In the VOF method, only the single continuity and momentum equations are solved for the entire domain. This approach is known as the "one-fluid" approach [126]. Therefore, the variables and material properties are defined as volume averaged of the two phases in each cell, as shown in equations (3) and (4)

$$\rho = \alpha\rho_1 + (1-\alpha)_{\rho_2} \quad (3)$$

$$\mu = \alpha\mu_1 + (1-\alpha)_{\mu_2} \quad (4)$$

The governing equations were solved with the finite-volume-based, open-source CFD toolbox, OpenFOAM (OpenCFD Ltd) [127,128]. The dispersed phase, water, flows into the micromixer from one inlet, while the continuous organic phase, e.g., Acetonitrile and ethanol, flows into the chip from the other inlet and mixes with the water. At the inlet, a zero-pressure gradient and constant velocity were used as boundary conditions. At the outlet, the velocity and volume fraction were set to be zero-gradient, and the pressure to be atmospheric.

2.4 3D printing of polypropylene microfluidic chips

3D-printed PP microfluidic chips were produced via fused deposition modeling (FDM) using an Ultimaker 3 printer (Ultimaker, The Netherlands). Both the developed devices were printed at a print speed of 25 mm/s with a nozzle temperature of 205 °C. The infill density was set at 100 % and the build plate was preheated at 85 °C after the application

of a polypropylene adhesion sheet (Ultimaker, The Netherland). The original STL file was converted to a print pattern using Ultimaker Cura 4.6.1 software (Ultimaker, The Netherlands). Alternating 50 μm thick layers were printed such that the pattern ran parallel to the length of the device, enabling leak-free and semi-transparent devices to be printed with PP. Probe needles were used to connect the chip with pump tubing. The effective dimensions of the microfluidic channels were evaluated using a digital microscope and then, a colored aqueous solution was run through the microchannels to confirm that the fluids were free to flow through the chips.

2.5 Microfluidic formulation of polymeric nanoparticles

For the preparation of PLGA NPs by microfluidics, the 3D printed chip was connected to two syringes mounted on two syringe pumps (Aladdin syringe pump, WPI Europe, Germany) through polyethylene tubing. A precise amount of PLGA alone or PLGA and CBD dissolved in acetonitrile was pumped against water at controlled flow rates and the samples were collected from the outlet of the chip. Two different final polymer concentrations were evaluated, *i.e.*, 5 and 10 mg/mL. The flow rate ratios (FRR) evaluated were 1:3 and 1:1 (ACN:water) and the total flow rates (TFR) were 10 and 12 mL/min. The amount of CBD added was 3 % w/w (Loading degree max 3%). The organic solvent was evaporated under a stream of nitrogen [129]. The specific experimental conditions used for the preparation of all NPs were defined according to the DoE reported in the method section 2.7.

2.6 Microfluidic formulation of liposomes

For the preparation of liposomes by microfluidics, the 3D printed chip was connected to two syringes mounted on syringe pumps (Aladdin syringe pump, WPI Europe, Germany) through polyethylene tubing. A precise amount of SPC and cholesterol or SPC, cholesterol, and CBD dissolved in ethanol was pumped against water at controlled flow rates, and the samples were collected from the outlet of the chip. Two different final lipids concentrations were evaluated, *i.e.*, 10 and 15 mg/mL. The FRR evaluated were 1:3 and 1:5 (ethanol:water) and the TFR were 10 and 12 mL/min. The amount of CBD added was 3 % w/w (Loading degree max 3%). The organic solvent was evaporated under a stream of nitrogen [129]. The specific experimental conditions used

for the preparation of all liposomes were defined according to the DoE reported in the method section 2.7.

2.7 Design of the experiments (DoE)

The effect of chip design and the preparation conditions (polymer/lipids concentration, FRR, and TFR) on NPs/liposomes size and polydispersity were evaluated by applying 2 levels full factorial design, characterized by 2^f experiments (where 2 is the number of levels and f is the number of factors) as reported in table 1.

Table 1. Two levels full factorial design matrix for the evaluation of the effect of chip design and preparation conditions

RUN	CHIP	CONCENTRATION	TFR	FRR
1	Z	-1	-1	-1
2	C	-1	-1	-1
3	Z	+1	-1	-1
4	C	+1	-1	-1
5	Z	-1	+1	-1
6	C	-1	+1	-1
7	Z	+1	+1	-1
8	C	+1	+1	-1
9	Z	-1	-1	+1
10	C	-1	-1	+1
11	Z	+1	-1	+1
12	C	+1	-1	+1
13	Z	-1	+1	+1
14	C	-1	+1	+1
15	Z	+1	+1	+1
16	C	+1	+1	+1

The design is characterized by a categorical factor, the chip design coded as Z (zigzag bas-relief) or C (split and recombine channels), and by three numerical factors, concentration, TFR, and FRR coded as -1 and +1. The numerical values of the coded variables are reported in table 2. The two nanocarriers were prepared by varying all the parameters within the same range with the only exception for the FRR. In this case, a larger range was selected since for values higher than 1:3 the preparation of the polymeric nanoparticles was not possible due to the precipitation of the polymer and chip clogging.

Table 2. Manufacturing condition and their corresponding numerical values of the coded variable

Coded Variable	NPs			Liposomes		
	Concentration	**TFR**	**FRR***	**Concentration**	**TFR**	**FRR***
-1	5 mg/ml	10 ml/min	0.33	5 mg/ml	10 ml/min	0.2
+1	10 mg/ml	12 ml/min	1	10 mg/ml	12 ml/min	0.33

* The FRR values used in the DoE represents the volumetric ratio of the organic and aqueous phases mixed through the microfluidic chip. Thus, the values of 0.2, 0.33, and 1 were used to numerically describe the FRR 1:5, 1:3, and 1:1 respectively.

All the NPs and liposomes prepared according to the DoE were characterized in terms of average particle size and polydispersity index as described in section 2.8. These two parameters represent the responses of the designs.

For each response, the two design were analysed by multilinear regression using a first order model:

$$y = \beta_0 + \sum_{i=1}^{n} \beta_i \cdot x_i + \sum_{i<j}^{n} \beta_{ij} \cdot x_i x_j$$

Where y is the response, β_0 is the model constant, β_i is the coefficient corresponding to the variables x_i (linear terms), and β_{ij} are the coefficients associated with the variables $x_i x_j$ (first-order interaction terms).

The goodness of fitting was evaluated through the adjusted coefficient of multiple determination (R^2_{adj}), while the residues analysis was used to test if the models meet the assumptions of the analysis. The ANOVA and coefficient analysis were instead used to identify the relative magnitude and the statistical significance of all the model terms.

The DoE design and analysis was carried out with the Minitab 18 statistical software (2017 Minitab, Inc.).

2.8 Nanocarriers physicochemical characterization

Prepared formulations were characterized for their average particle size (Z-average) and polydispersity index (PDI) by dynamic light scattering (DLS) using a Malvern Zetasizer Nano S instrument (Malvern Instruments Ltd, UK).

The encapsulation efficiency was evaluated with a direct ultracentrifugation method. Briefly, a precise amount of nanocarriers was ultracentrifuged at 70000G for 1 hour and then the pellet was dissolved with acetonitrile. The obtained solution was analyzed by HPLC to evaluate the content of CBD.

2.9 HPLC method for the analysis of CBD

The content of CBD was assessed by high-performance liquid chromatography (HPLC Agilent 1260 Infinity II, Agilent, USA) using an isocratic mixture of 0.5 % formic acid in water and 0.5 % formic acid in acetonitrile (ratio 15:85) as mobile phase, with a flow rate of 1 mL/min in an Agilent Poroshell 120 EC-C18, 100x4.6 mm, 2.7 μm column (Agilent, USA). The injection volume was 20 μL and the detection signal was recorded at 220 nm keeping the analysis system at room temperature.

2.10 Statistics

The data presented are the mean ± standard deviation of triplicate measurements and are representative of at least three independent experiments.

3. RESULTS AND DISCUSSION

3.1. Microfluidic chips development

The development of a 3D printed object starts from the computer assisted design (CAD) of the model. Microfluid chips can be engineered with active or passive micromixing depending on the characteristics needed. Active micromixing requests a higher complexity and the presence of an external source of energy such as ultrasounds or magnetic fields. On the contrary, passive micromixing does not need any external energy source because it takes advantage of the presence of perturbations in the microchannels such as bas-relief, splits, 3D structures that induct a chaotic advection effect. These modifications in the microfluidic channels help to increase the contact surface and contact time between the species by splitting, stretching, folding, and breaking the flows [34,38,121].

In this work, we developed two different micromixing designs with a “zigzag 3D structure” and a “split and recombine circular sub-channels”.

Figure 1A represents the 3D design of the zigzag chip (Z chip) which has two inlets that are combined with a T-junction into the main channel. The main channel presents the zigzag 3D structure along all its length to induce the desired chaotic mixing. The channels of this chip present a square section with a side of 1 mm while the zigzag structure has a height of 500 µm. The total length of the main channel is 60 mm.

Figure 1B represents the second microfluidic design which takes advantage of split and recombine sub-channels (C chip). Also, in this case, it presents two squared inlets (1 mm side) combined with a T-junction into the main channel. The subsequent circular splitting is repeated six times and kept unequal to have a difference in the velocity of the fluids and therefore unbalanced collisions of the fluid streams [130]. The major sub-channel has a side of 600 µm while the minor sub-channel has a side of 400 µm both with a square section.

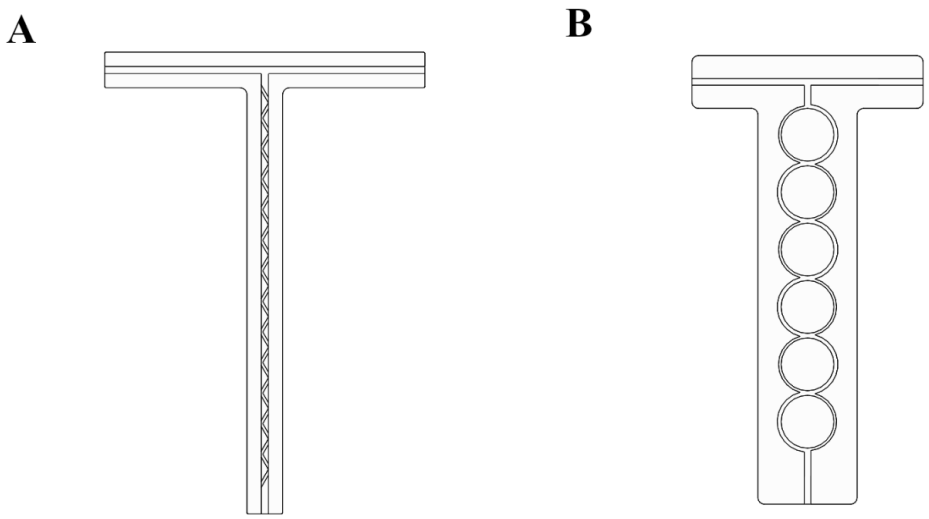

Figure 1. Computer aided design models of A) "Z" (zigzag design) microfluidic chip and B) "C" (Split and recombine design) microfluidic chip.

These two models were evaluated with computational fluid dynamic (CFD) studies to assess the effective micromixing potentiality. Acetonitrile and ethanol were selected as the organic phase against water in the two inlets of each microfluidic chip. These two solvents were selected to produce PLGA NPs and liposomes respectively. The inlets and outlet have been assigned uniform velocity profile and zero static pressure as boundary conditions. The density of water, ethanol, and acetonitrile are 9.97 x 10^2, 7.89 x 10^2, and 7.86 x 10^2 kg/m^3, respectively. FRR 1:3 and 1:1 were evaluated for

ACN:water (PLGA NPs) meanwhile FRR 1:3 and 1:5 were evaluated for ethanol:water (Liposomes).

Figure 2 shows the distribution of the volumetric fraction of each solvent (ACN:water) with an RGB scale.

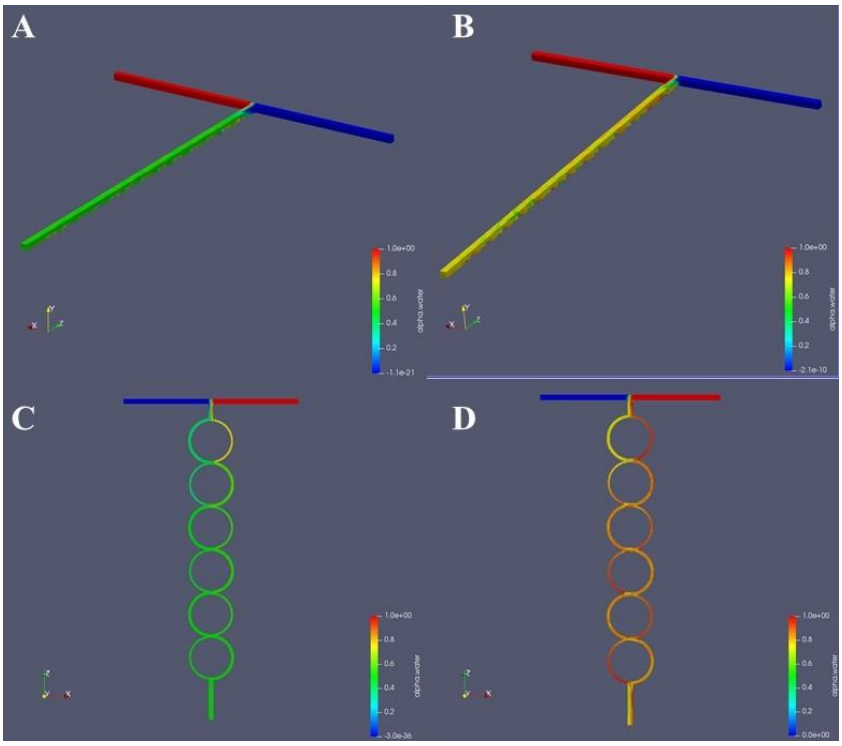

Figure 2. Computational fluid dynamic simulation of Z and C chips with water and ACN. The distribution of the volumetric fraction of each solvent is represented with an RGB scale. A and B show Z chip at FRR 1:1 and 1:3, respectively. C and D show C chip at FRR 1:1 and 1:3, respectively. The red color is for water and blue color is for ACN.

These results demonstrate that the developed microfluidic chips present an effective mixing performance. In particular, the mixing was more effective at FRR 1:1 (Figure 2A, C) for both chips reaching a complete mixing after 0.79 sec in the Z chip (Figure 2A) and after 1 sec and 3 circular sub-channels in the C chip (Figure 2C). At FRR 1:3 (Figure 2B, D), the mixing performance was lower reaching a complete mixing only at the end of the microfluidic chip (1.97 sec in the Z chip and 1.6 sec in the C chip). FRR 1:5 results are not shown since this parameter brought to chip occlusion due to polymer precipitation during the manufacturing of the NPs.

Figure 3 shows the distribution of the volumetric fraction of each solvent (ethanol:water) with an RGB scale.

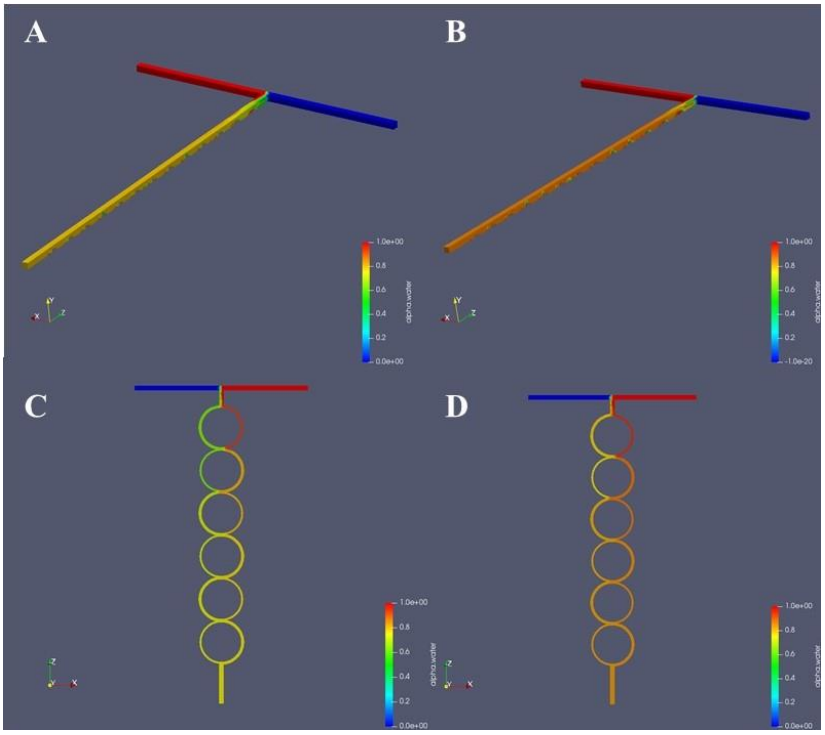

Figure 3. Computational fluid dynamic simulation of Z and C chips with water and ethanol. The distribution of the volumetric fraction of each solvent is represented with an RGB scale. A and B show Z chip at FRR 1:3 and 1:5, respectively. C and D show C chip at FRR 1:3 and 1:5, respectively. The red color is for water and blue color is for ethanol.

Even in this case, the mixing performance was effective at both the FRR evaluated (1:3 and 1:5) confirming a potential to produce lipidic nanocarriers. The complete mixing of the two fluids was reached with all the conditions studied in less than 1.9 sec (Figure 3 A 1.41 sec, B 1.87 sec, C 1.49 sec, D 1.49 sec).

According to these results, the two chips were printed using polypropylene as printing material. This polymer was selected because of its chemical resistance to commonly used microfluidic solvents such as ACN, ethanol, acetone, and methanol [37] compared to the polylactic acid (PLA) commonly used to print objects with the FDM technique. During the manufacturing of the chips, the effective channel dimensions were evaluated with a digital microscope (Figure 4A Z chip, Figure 4B C chip) showing an accordance with the dimension of the CAD project and thus confirming the optimal printing resolution. After the manufacturing of the two chips, a colored aqueous solution was run through the microchannels to confirm that the fluids were free to flow through the chip (Figure 4C, D).

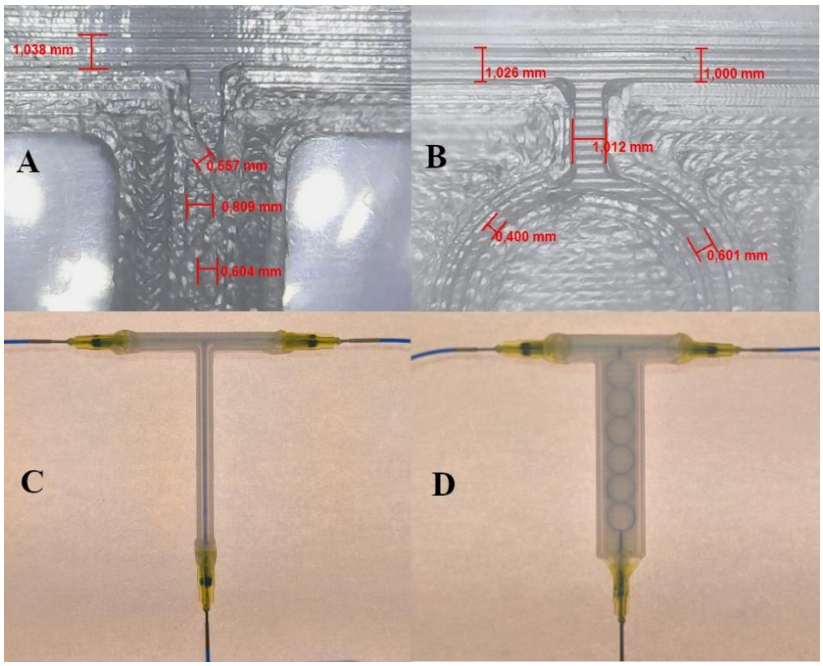

Figure 4. Printed channels measure of Z chip (A) and C chip (B). In the Z chip it can be observed the zigzag structure meanwhile in the C chip it is notable the asymmetric dimensions of the splitted channels. C and D show a colored aqueous solution running through the two printed chips.

3.2 Nanocarriers manufacturing and evaluation of the influence of microfluidic parameters

The two 3D-printed microfluidic chips were utilized to produce both polymeric and lipidic nanocarriers. PLGA and SPC/cholesterol were selected as model excipients as they have been already widely utilized in the production of polymeric NPs and liposomes, respectively.

To evaluate as the different microfluidic parameters and the chip design affect the two types of prepared nanocarriers it has been decided to perform a factor influence study applying a 2-level factorial design [131]. Once all the experimental runs provided by the DoE (table 1) were carried out and the samples characterized, it has been performed a preliminary assessment of the obtained data plotting them in an individual value plot (Figure 5). Interestingly, NPs and liposomes appear completely different, with the first showing a much wider size and polydispersity distributions with a higher median value for the size compared with the latter.

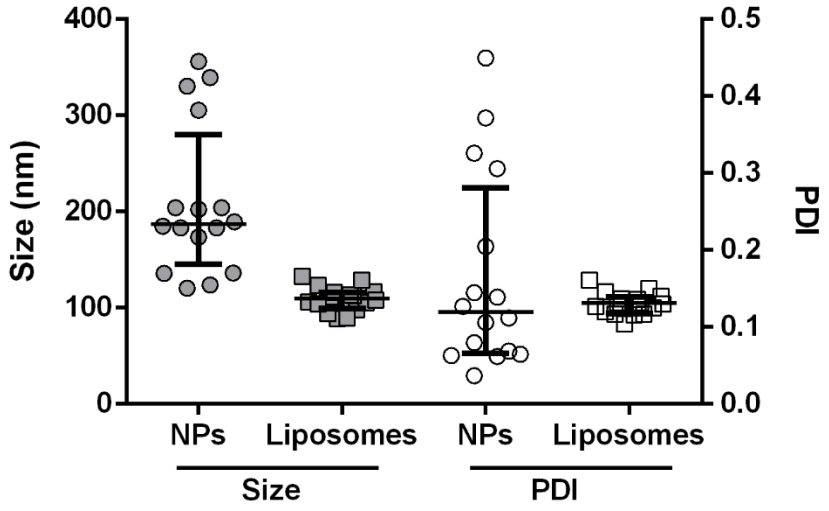

Figure 5. Individual value plot of z-average diameter and PDI. The lines above each group represent the median (central line) and the interquartile range (distance between the two outer lines).

Such results could be intrinsic to the two nanocarriers but could also be due to the FRR, which for practical reasons (Polymer precipitation and consequent chip occlusion with FRR 1:5), is the only preparation variable applied in different range for NPs and liposomes (from 1:1 to 1:3 and from 1:3 to 1:5 for NPs and liposomes. respectively). To verify this hypothesis, the size and PDI of NPs and liposomes prepared at the same FRR (1:3) were compared with the t-test. The results indicate statistically significant differences and consequently the differences observed in figure 5 cannot be attributed to the different FRR range used (Supplementary figure 1). Another preliminary evaluation concerns the check of any correlation between the two responses (size and PDI) for each nanocarrier. Pearson correlation analysis has been performed and the results, once again, are specific for NPs and liposomes (Supplementary figure 2). In fact, while for liposomes no correlation was observed, for NPs size and PDI show a strong positive correlation (Pearson coefficient equal to 0.932 with a P-value lower than 0.001).

The size and PDI values were then analyzed through multilinear regression to assess the influence of all the experimental variables. The results of DoE analysis are summarized using Pareto plots and "main effect" and "interaction" plots [132] while all the detailed results, goodness of fit statistic, residual analysis, ANOVA, and coefficient analysis are reported in the supplementary materials. The fitting procedure of PDI values for liposomes resulted to be poor (R^2_{adj} lower than 0.2 and non-significant model

regression), suggesting as such a value are not influenced by the four-variable studied or the mathematical model is not adequate. For this reason, the PDI of liposomes will not be more discussed subsequently. The Pareto plots reported in figure 6 show which variables have a statistically significant effect on the NPs and liposomes features. Interestingly, NPs and liposomes show different behaviour concerning the role of the preparation parameters. In fact, even if the polymer and lipid concentrations represent a crucial parameter for the preparation of both nanocarriers, the size of liposomes depends also on the chip design while that of the NPs are strongly affected by the FRR and the interaction between FRR and concentration. Another noteworthy aspect concerns the fact that the TFR does not exert any effect both on NPs and liposomes, at least within the range analysed. Moreover, the Pareto plots as well as the Anova and coefficient analysis reported in the supplementary materials demonstrate as the results for the size and PDI of NPs are equivalent, confirming that these two parameters are strongly correlated.

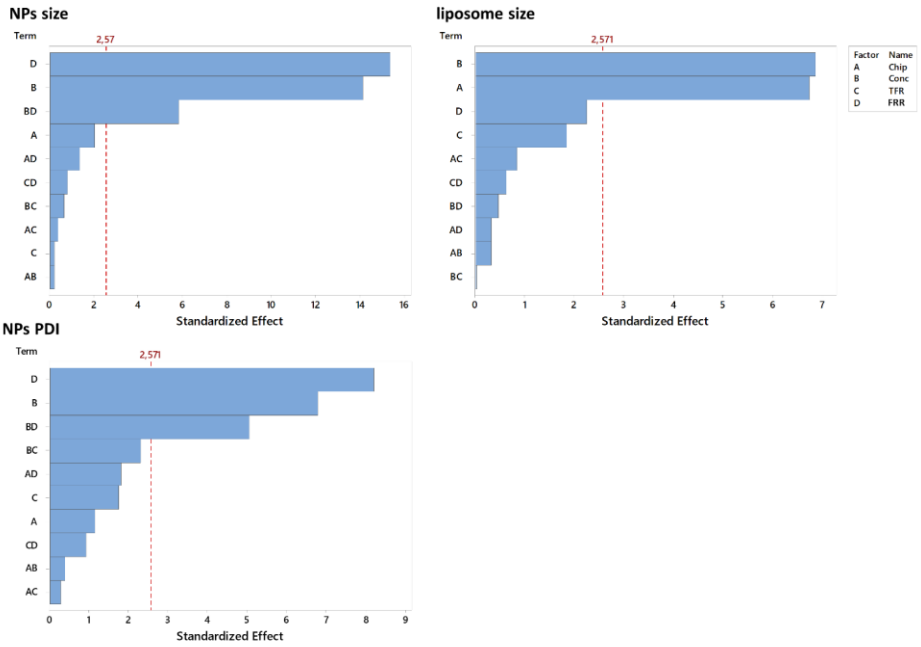

Figure 6. Pareto plots for the size of the NPs (Upper left panel), for the PDI of the NPs (lower left panel), and for the size of liposomes (upper right panel). The red line represents the statistically significance limit (the t-values corresponding at a one-sided probability of 0.025 from a t distribution with the same degree of freedom of the error term) when the relevance of a variable is reported as standardized effect (t-value of the coefficient).

The Pareto plots show the relevance of the investigated factors and their significance; however, the use of the "main effect" and "interaction" plots provides a more detailed picture of how significant factors influence responses [132]. The main effects and interaction plots in figure 6 refer only to the factors that resulted statistically significant from the Anova and coefficient analyses. For both nanocarriers, the use of a higher polymer or lipid concentration determines a size increase (and also an increase of the PDI for NPs). For the liposomes, a marked size increase is observed also moving from Z to C chip while in the NPs preparation an increase of the FRR produces much smaller particles. Interestingly, for each nanocarrier all the significant parameters possess an effect of comparable magnitude, determining a size variation with respect to average value of around 7% for liposomes and 24% for NPs. Finally, during the NPs preparation, a significant effect is also due to the interaction between concentration and FRR (upper right panel in figure 7). Specifically, the effect of the increase of concentration is much more relevant when a lower FRR (greater volume of the water phase) is applied.

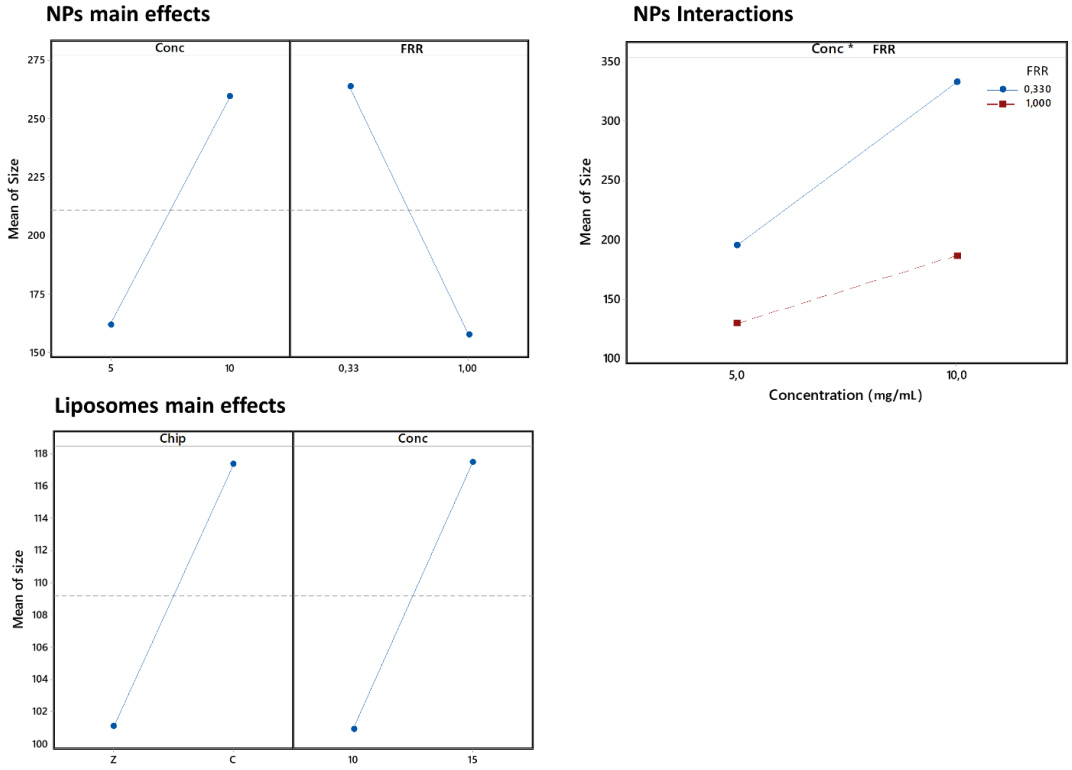

Figure 7. Main effect plots for the size of the NPs (Upper left panel) and liposomes (lower left panel), and interaction plot for the size of the NPs (upper right panel).

These DoE results are important to evaluate how the production parameters influence the final formulation manufactured with the 3D printed microfluidic chip. As usual, each formulation needs to be optimized with specific parameters since it is impossible to obtain a universal set of values that are efficient for every nanosystem.

3.3 Effect of CBD encapsulation on nanocarriers manufacturing

The DoE allowed understanding how the different experimental parameters affect the unloaded nanocarriers' size and size distributions as a function of the chip design. The next step is to evaluate the eventual effect of an encapsulated drug. As a model drug, we selected CBD, an active molecule with a growing interest in the pharmaceutical field with different applications in a large number of diseases such as dermatological problems, cancer, psychiatric disorders, microbiological infections, and other [133–136]. The CBD was encapsulated in NPs and liposomes using both chips at the experimental conditions giving the highest and lowest size according to the results of DoE analysis. Such experimental conditions were obtained using the linear partial desirability functions that maximize and minimize the response (size) and are reported in the supplementary materials (Supplementary table 1).

The comparison between size and PDI for unloaded and CBD-loaded nanocarriers is reported in figure 8. The presence of the CBD has a marginal or null effect on the features of NPs and liposomes, which therefore still depend on the experimental preparations parameters as identified with the factorial design analysis.

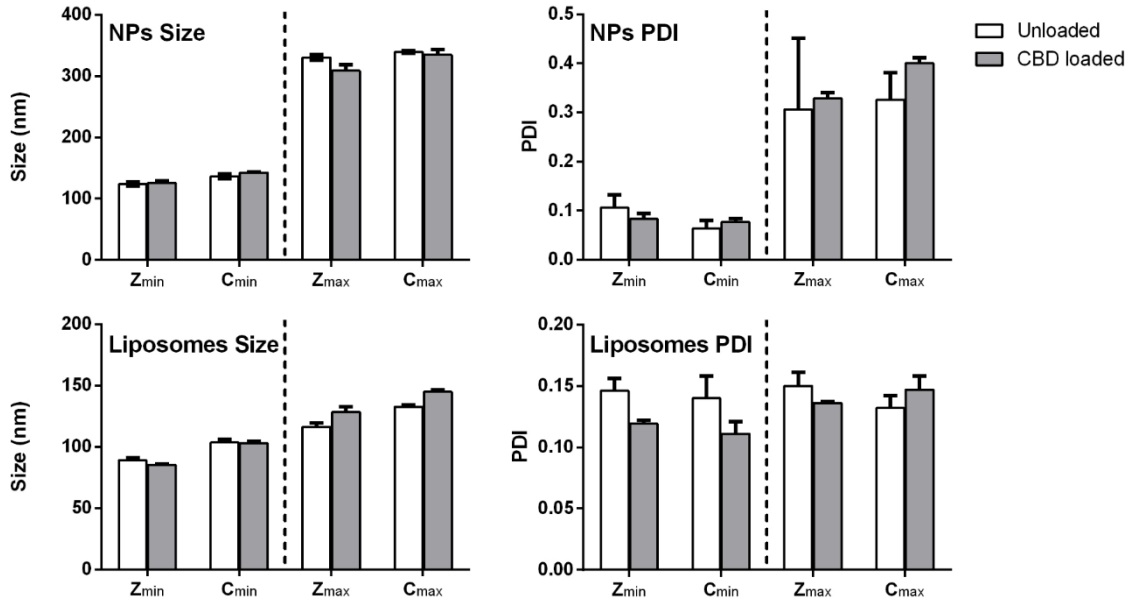

Figure 8. Comparison between the Size and PDI of unloaded and CBD-loaded NPs and liposomes. The x-axis reports the experimental conditions applied where Z and C refer to the chip design and the subscript max or min to the combination of parameters concentration, TFR, and FRR that maximize or minimize the size (the numerical values in supplementary table 1).

For the loaded nanocarriers, it has been also determined the encapsulation performance of CBD. As the amount of CBD was 3% w/w on excipient weight, it was selected the loading degree (LD%) as the most suitable parameter for evaluating encapsulation, since it is independent from the amount of drug added in each formulation. For each prepared nanocarrier, the LD% can range from 0 (no CBD encapsulated) to 3 (all the added CBD is encapsulated). The results of the LD% (Figure 9) highlight a different behavior between NPs and liposomes. While for the lipid carriers the LD% appears almost independent of the preparation conditions, for NPs the LD% is strongly affected by them and particularly it seems correlated with the size of the particles. The LD results within each type of nanocarriers were further tested using one-way Anova followed by Tukey test. The results of this type of analysis indicated as there were no statistically differences for the LD% for all liposomes batches. Interestingly, the LD% of NPs showed a variation statistically significant only as a function of the experimental conditions used (max or min) but not as a function of the chip design (Z or C).

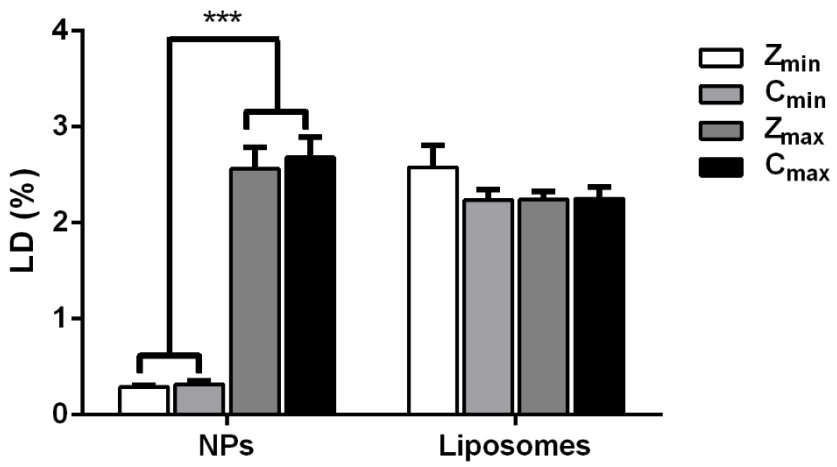

Figure 9. LD% for all the CBD-loaded NPs and Liposomes. The asterisks refer to the the p-value calculated during the post hoc pairwise comparison (Tukey test): * $0.05 < p < 0.01$; ** $0.01 < p < 0.001$; *** $p < 0.001$. The absence of asterisks means a $p > 0.05$.

4. CONCLUSIONS

In this work, simple, easily manufactured 3D printed microfluidic devices have been evaluated. The two developed chips resulted effective to produce model polymeric and lipidic nanocarriers. Thanks to additive manufacturing technology, microfluidics became more accessible to researchers around the world. Our two microfluidic chips STL files are available as supplementary material to be readily printed and used. This has the potential to widen accessibility further by eliminating the design barrier in addition to the fabrication barrier largely limiting access to microfluidic technology at present. Every formulation that takes advantage of microfluidic manufacturing needs to be developed with appropriate microfluidic parameters to reach the desired physicochemical characteristics, and the most influent parameters can be evaluated by DoE as done in this work.

To the best of the author's knowledge, 3D printed PP based microfluidic devices have not previously been realized by FDM printing for the manufacturing of nanocarriers. This is a first approach to this opportunity that can lead to further designs to improve the characteristics of the microfluidic system. The compromise between resolution and material choice will certainly continue to define the preference for either technology.

Part IV

The content of part IV has already been published in: J. Drug Deliv. Sci. Technol. 65 (2021) 102661. https://doi.org/10.1016/j.jddst.2021.102661

AN EASY 3D PRINTING APPROACH TO MANUFACTURE VERTICAL DIFFUSION CELLS FOR *IN VITRO* RELEASE AND PERMEATION STUDIES

ABSTRACT

Vertical diffusion cells are utilized in the pharmaceutical and cosmetic fields to study the release and permeation of active ingredients through polymeric or biological membranes. Nevertheless, the commercially available glass-based systems are expensive and need to be carefully handled due to their fragility. Fusion deposition modeling 3D printing is an additive manufacturing technique that allows producing objects by printing layer over layer different thermoplastic materials. Among them, polypropylene is a robust, flexible, and chemically inert polymer that can resist to many organic solvents and to heating. In this work, we designed and printed a vertical diffusion cell following pharmacopeia requirements by using polypropylene in a fused deposition modeling 3D printer. The model was developed to fit in a heating block to avoid the use of warm water recirculating system.

The vertical diffusion cells were leak-free and presented chemical resistance and no interaction with the tested molecules (*i.e.*, caffeine, diclofenac sodium, and glycyrrhetinic acid). The 3D printed cells were compared to commercially available glass cells and then two different types of synthetic membranes (*i.e.*, PDMS and Strat-M®) were used to evaluate the permeation of a caffeine hydrogel.

The developed 3D printed testing system could represent an efficient alternative to the glass-based equipment.

Keywords: 3DP; fusion deposition modeling (FDM); Franz cells; VDCs; polypropylene (PP); polymeric membranes.

1. INTRODUCTION

During the last few years, 3D printing (3DP) continued to grow as an innovative additive manufacturing (AM) technology with applications in many different areas including pharma [4,137]. Recently, many pharmaceutical applications have been published in the literature reporting the production of dosage forms (i.e., tablets, capsules, suppositories, and vaginal rings), testing systems (i.e., ocular, nasal, and respiratory models), and manufacturing devices (i.e., microfluidic chips) [6,8,138,139]. Among the 3D printing techniques, fused deposition modeling (FDM) presents several advantages including relatively inexpensive printers and materials, low maintenance costs, a large selection of commercially available materials, the ease of initial use, and the ability to start, stop, and integrate complexity on the fly [33].

Taking advantage of this technology, the acronyms DIY (Do-It-Yourself) is gaining attention over research laboratories. The additive manufacturing techniques allow researchers to develop and produce almost any kind of object needed in the laboratory from the simplest to even more complex ones with a real decrease in costs [140,141].

In the pharmaceutical and cosmetic fields, vertical diffusion cells (VDCs or Franz cells) are routinely used for the study and analysis of both release and permeation of active molecules from different formulations through the use of polymeric and biological membrane [40]. These kinds of studies are important since they can determine the feasibility of delivering the cargo to and through the skin [43].

Conventional VDCs are typically manufactured from glass and they can be found in the market in many shapes, sizes and may be modified depending on the required experimental conditions. According to United States Pharmacopeia (USP, www.uspnf.com, Topical and transdermal drug products), the VDC assembly consists of two chambers (donor and receptor), separated by a membrane. Commonly, this system is used for testing the *in vitro* release rate of topical drug products such as creams, gels, and ointments. Even alternative diffusion cells that conform to the same general design can be used and can be made from any materials that do not react with or absorb the test product or samples. Commercial VDCs are commonly made from borosilicate glass that results fragile and require careful handling during their utilization. Only one 3D printing approach was considered in the literature to produce VDCs using stereolithography (SLA) [142]. This additive manufacturing technique requires the

utilization of acrylate-based resins which are photopolymerized during the printing procedure and then they need to be post-cured to obtain the final object. Moreover, the type of resin utilized presented physical and chemical interactions with the tested drug, requiring a plastic coating to avoid these problems.

FDM, in comparison to SLA, is easier to use, it has lower overall production costs and it does not need post-curing after printing. Another important aspect to consider is that the selection of thermoplastic FDM printing materials is very wide and the most appropriate one can be chosen depending on the needs.

In this work, we developed an alternative 3DP vertical diffusion cell using polypropylene (PP) as manufacturing material in a FDM printer. This material was selected since it is a robust, flexible, and chemically inert polymer that can resist to many organic solvents and to heating [37]. The 3DP VDCs were tested for leaking and then were compared to glass VDCs to evaluate the potential applicability.

In the *in vitro* permeability studies, different membranes can be used including human skin, animal skin as well as polymeric membranes. However, biological membranes have limitations such as cost and availability of human skin and ethical consideration for the use of animal skins. Besides, compared to synthetic membranes, biological models exhibit high variability that complicates the experimental design, statistical significance, and number of replicates required [143]. Moreover, biological models possess a short half-life, special storage requirements, higher costs, and safety issues [112].

For our work, we selected skin-mimicking membranes (Strat-M®) which comprise two layers of polyethersulfone on top of one layer of polyolefine. These membranes possess a porous structure that imparts additional skin-like properties by creating a gradient across the entire thickness [144].

Finally, Strat-M® membranes were compared with polydimethylsiloxane (PDMS) membranes [145], using a caffeine hydrogel as model formulation since this active is a hydrophilic molecule widely used in topical applications [146].

2. MATERIALS AND METHODS

2.1 Materials

Neutral polypropylene 3D printing filament was kindly provided from Verbatim (Italy). Caffeine was kindly provided by BASF (Germany), diclofenac sodium was obtained from Farmalabor (Italy), glycyrrhetinic acid, and xanthan gum were purchased from A.C.E.F. (Italy). Strat-M® membranes were obtained from Merck (Germany), 250 µm thick polydimethylsiloxane (PDMS) membranes were kindly provided by Shielding Solutions Limited (Essex, UK), Spectra/Por™ 7 Standard RC dialysis membranes (6-8 kDa cut-off) were purchased by Spectrum Labs (USA). All the other solvents used were HPLC grade.

2.2 Design and development of the VDCs

The original 3D model project was designed using the free online computer aided design (CAD) tool Tinkercad® (Autodesk, USA). The cell was designed to fit in a heating block (IKA, Germany) used to control the temperature during experiments. The cell is composed of a receptor part in which is present a withdrawal window with its cap, two donor compartments depending on the origin of the formulation, liquid or semisolid, and a stirring block useful to adjust the receptor volume. The 3D printed stirring block presents a slot to insert a magnetic stirring bar. The 3DP VDCs present a receptor compartment volume of 9 or 11.5 mL (with or without stirring block respectively) and an effective diffusion area of 1.583 cm^2. The files were exported from the online CAD software as STL (Stereolithography interface format) to be then converted into machine language with a computer aided manufacturing (CAM) software (STL files provided in the supplementary material).

2.3 Manufacturing process of the 3D printed VDCs

3D-printed PP VDCs were produced via fused deposition modeling (FDM) using an Ultimaker 3 printer (Ultimaker, The Netherlands). The VDCs were printed at a print speed of 25 mm/s with a nozzle temperature of 205 °C. The infill density was set at 100 % and the build plate was preheated at 85 °C after the application of a polypropylene adhesion sheet (Ultimaker, The Netherland). The original STL file was converted to a print pattern using Ultimaker Cura 4.7 software (Ultimaker, The Netherlands). Layer

thickness was set to 150 μm enabling the production of leak-free PP VDCs. The 3DP VDCs were tested for leaks by filling both compartments with water. The receptor compartment and the donor compartment were ulteriorly sealed with the application of laboratory sealing film. The system was examined for leaks over a minimum of 24 hours and it was considered good if no water was present on the outer wall after this period.

2.4 Compatibility studies of the 3D printed VDCs

To assess the compatibility of the VDCs with active compounds, three different model drugs were evaluated, *i.e.*, caffeine (2 mg/mL water solution), diclofenac sodium (2 mg/mL water solution), glycyrrhetinic acid (0.02 mg/mL 50% ethanolic solution). The solutions were prepared and used to fill the receptor compartment of the cell that was then closed using laboratory sealing film and warmed up at 32 °C together with 400 rpm magnetic stirring. After 24 hours, the concentration in the receptor compartment was compared with the initial concentration to confirm that any amount of drug was retained or adsorbed from the cell wall.

The amounts of the model drugs were measured by HPLC (1260 Infinity II, Agilent, USA) using a mixture of 0.5% formic acid in water and methanol (ratio 60:40 for caffeine, 30:70 for diclofenac sodium, and 5:95 for glycyrrhetinic acid) as mobile phase, with a flow rate of 1 mL/min in an Agilent Zorbax Eclipse Plus C18, 150 x 4.6 mm, 5 μm column (Agilent, USA). The injection volume was 20 μL and the detection signals were recorded at 275 nm (caffeine and diclofenac sodium) and 276 nm (glycyrrhetinic acid) keeping the analysis system at room temperature.

2.5 *In vitro* release comparison: glass vs polypropylene 3D printed VDCs using a caffeine hydrogel

A comparison between commercial glass VDCs and 3DP VDCs was performed using a cellulose-based dialysis membrane (6-8 kDa cut-off, Spectra/Por 7 Standard RC Dry Dialysis Tubing, Spectrum Labs, USA). The selected model formulation was a caffeine hydrogel composed of caffeine (5 mg/mL), xanthan gum (0.5% w/v), and water.

The glass VDCs (Teledyne Hanson Research, USA) presented a receptor compartment volume of 7 mL and an effective diffusion area of 1.766 cm^2 meanwhile the 3DP VDCs

were utilized with the stirring block presenting a receptor volume of 9 mL and an effective diffusion area of 1.583 cm^2. Water was used as receptor medium in both cell types. The receptor medium was continuously stirred at 400 rpm. The glass system was thermostated at 32 ± 1 °C with a circulating jacket meanwhile the 3DP system was thermostated at 32 ± 1 °C with a heating block positioned over a heating plate. The efficacy of heat transfer and temperature control between the heating plate and the receptor medium inside the 3DP cell was previously assessed by measuring the temperature with a thermometer. At predetermined sampling intervals (0.5, 1, 2, 3, 4, 5, 6, and 24 h), samples were withdrawn from the receptor compartment and replaced with an equal volume (0.2 mL) of fresh buffer. The content of the active compound in each sample was then determined by HPLC as reported above. A calibration curve of caffeine was performed with a concentration ranging from 0.01 to 0.5 mg/mL obtaining a correlation coefficient (R2) of 0.9997.

The amounts of the active compound released at each time point (AR_{tn}) were obtained using the eq. (1) for the first time point and eq. (2) for the subsequent time points:

$$AR_{t_1} = \frac{C_{t_1} * 1000 * V_c}{A_o} \qquad (1)$$

$$AR_{t_n} = \frac{C_{tn} * 1000 * V_c}{A_o} + \left(AR_{t_{n-1}} * \frac{V_s}{V_c}\right) \qquad (2)$$

where AR (µg/cm^2) is the amount released at t_n sampling interval, the C_t (mg/mL) is the concentration of caffeine determined at t_n sampling interval, V_c (mL) is the volume of diffusion cell receptor compartment, A_0 (cm^2) is the cell diffusion area and V_s (0.2 mL) is the sampling aliquot volume.

2.6 *In vitro* permeation studies using 3D printed VDCs with different membrane models

Permeation studies using the PP 3DP VDCs were conducted using a caffeine hydrogel (5 mg/mL, 0.5% xanthan gum) applied to two different membranes, *i.e.*, skin mimicking Strat-M® membranes and 250 µm thick PDMS membranes. The skin-mimicking Strat-M® membranes are composed of two layers of polyethersulfone on top of one layer of

polyolefine. These polymeric layers create a porous structure with a gradient across the membrane in terms of pore size and diffusivity. The porous structure is impregnated with a proprietary blend of synthetic lipids, imparting additional skin-like properties to the synthetic membrane [93]. PDMS membranes were selected as model membranes, already used in other studies, with a lower permeation compared to dialysis membranes [142,147,148].

The receptor chambers were filled with water kept continuously stirred at 400 rpm. The system was thermostated at 32 ± 1 °C with a heating block positioned over a heating plate. At predetermined sampling intervals (0.5, 1, 2, 3, 4, 5, 6, 24 h), samples were withdrawn from the receptor compartment and replaced with an equal volume (0.2 mL) of water. The content of caffeine in each sample was determined by HPLC with the method reported above. Equations 1 and 2 were utilized to calculate the amount of active compound released at each time point.

2.7 Statistics

The data presented are the mean ± standard deviation of triplicate measurements and are representative of at least three independent experiments.

3. RESULTS AND DISCUSSION

3.1 Design, 3D printing, and compatibility studies of the vertical diffusion cells (VDCs)

The CAD design of the 3DP VDCs was developed following the USP guidelines presenting a receptor and a donor compartment (Figure 1).

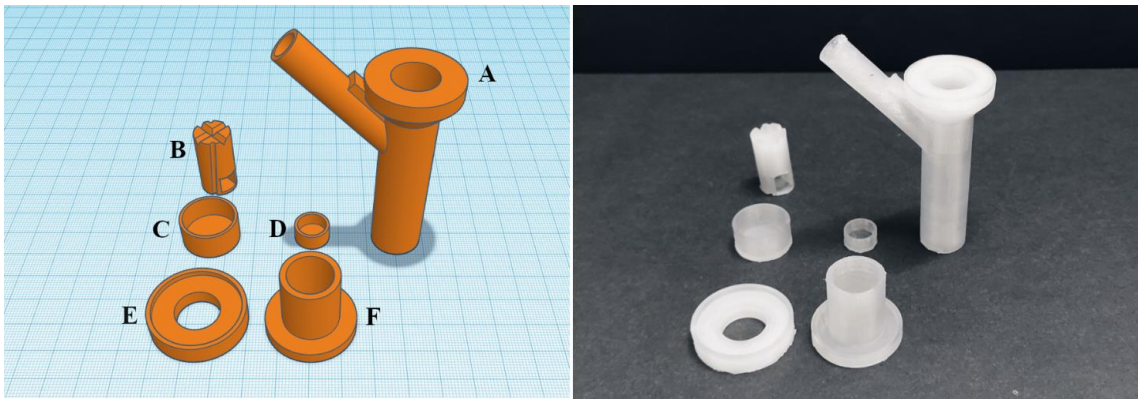

Figure 1. CAD design of the VDC parts and polypropylene 3D printed parts. A) Receptor compartment with withdrawal window; B) Stirring block; C) Cap for donor compartment for liquid formulations; D) Cap for withdrawal window; E) Donor compartment for semisolid formulations; F) Donor compartment for liquid formulations.

These two sections are separated by a membrane (*e.g.*, synthetic or biological) that allows the permeation of the tested molecule. The material selected to print out the entire system was polypropylene since it is a robust, flexible, and chemically inert polymer.

This last property is the most important to meet the pharmacopeia requirements since the cell material does not have to interact chemically and/or physically with the compound analyzed. This is also the reason because VDCs are traditionally made from glass that is a material known for its lack of interaction with active ingredients [149]. The drawbacks of this material are mainly its fragility and the high production costs. Taking advantage of FDM 3D printing, it was possible to print a VDC with a low cost and without fragility since PP results robust and flexible. The printed cell resulted semitransparent with the possibility to examine the receptor medium for the presence of air bubbles. The printed layers fusion was evaluated to prevent eventual leakage. The receptor and the donor compartments were filled to the top with water and sealed with

laboratory film. After 24 hours no leakages were detected from the VDCs confirming the effective fusion of the layers produced with the FDM technique.

Then, another important step was to evaluate the compatibility of the material with active molecules even if PP is already known for its chemical resistance. Authors were more worried about eventual physical absorption into spaces between layers. We tested three different molecules varying their chemical nature: caffeine was selected as amphiphilic molecule, diclofenac sodium as salt, and glycyrrhetinic acid as hydrophobic molecule. These molecules in their respective solutions were used to fill the receptor compartment for 24 hours and the analysis of concentration after this period showed no differences with the initial concentration confirming the compatibility with these active molecules. As it is impossible to test every type of molecule, we choose these three as models, but we suggest assessing the compatibility of each specific active compounds before utilizing it in an *in vitro* permeation test with the 3D printed VDCs.

3.2 *In vitro* release and permeation studies

In vitro release studies were performed first in both glass and 3DP VDCs to evaluate effective comparability between the two systems. A commonly used cellulose dialysis membrane was applied to divide the receptor from the donor compartment and a caffeine hydrogel was utilized. This comparison showed no significant differences in the release of the active molecule with the 3DP VDCs when compared with the glass VDCs as shown in figure 2 confirming the suitability of the developed 3DP system. Release studies with the 3DP VDCs resulted in 1164 ± 36 µg/cm^2 of caffein permeated in the receptor compartment after 24 h meanwhile the release was 1123 ± 41 µg/cm^2 for the glass homologues.

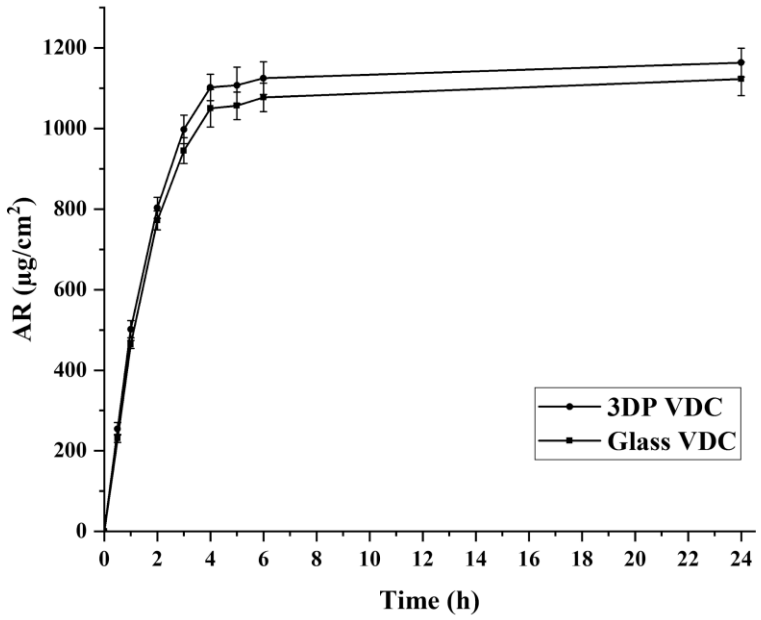

Figure 2. Comparison between glass VDCs and the 3DP VDCs using a cellulose dialysis membrane (6-8 kDa cut-off) and a 5 mg/mL caffeine hydrogel.

After the assessed suitability of the 3DP VDCs, two different membranes were employed for a permeation study using a caffeine hydrogel. Excised human and animal skins are often utilized to study skin permeation profiles of topical formulations, however, they are expensive and possess several drawbacks. Among them, there are variations of skin thickness, diseased skin states, preparation complexity, age of the donor, the density of hair follicles, and skin storage conditions that can hinder reproducibility data [112,143].

In this study, we decided to compare standardized synthetic Strat-M® membranes as a reproducible alternative to excised human skin [143] and 250 µm thick PDMS membranes as a low permeability model membranes (Figure 3) [150].

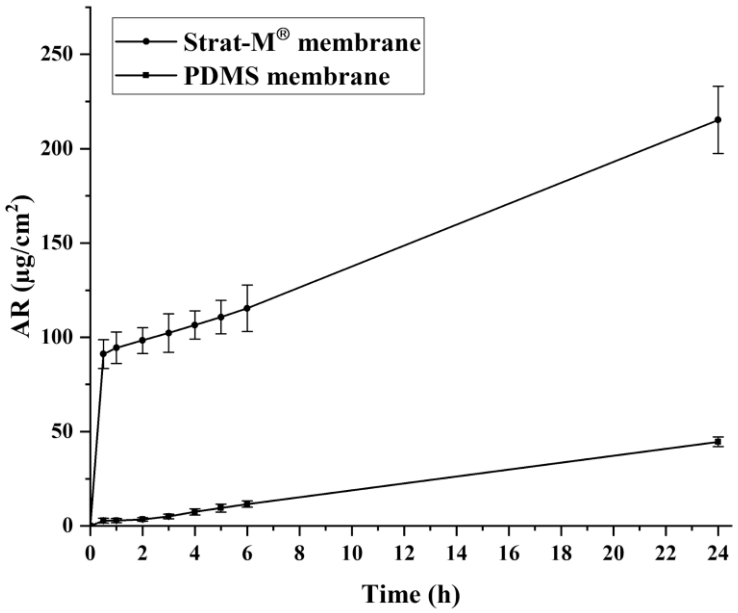

Figure 3. Comparison between Strat-M® and PDMS membranes using the 3DP VDCs and a 5 mg/mL caffeine hydrogel.

The drug permeation resulted higher with the Strat-M® membranes with an amount permeated after 24 h of 215 ± 18 µg/cm^2 meanwhile for the PDMS membranes, the drug permeated was more than 4 times lower (44.6 ± 2.6 µg/cm^2). Since this membrane is made with a hydrophobic material, the permeation through it is influenced by the nature of the tested molecule. Since caffeine result hydrophilic, its passage through this type of membrane resulted very low even after 24 hours.

In release studies, mathematical models play a crucial role in evaluating the drug release mechanism [60]. In these studies, the release profile of the drug from the xanthan gum hydrogel resulted linear with the time for the utilized membranes confirming zero-order kinetics (Strat-M® R^2 0.9972; PDMS R^2 0. 9974) [151].

4. CONCLUSIONS

In this work, we successfully developed a 3D printed VDCs model useful for the evaluation of *in vitro* drug release and permeation. The design was in accordance with the pharmacopeia requirement and the dimensions were studied to perfectly fit in a heating block to control the temperature avoiding warm water recirculatory system. As the system has been developed for 3D printing it is possible to continue the

personalization based on the needs for example changing or reinventing the donor compartment. The material employed for the manufacturing of the cell (*i.e.*, polypropylene) confirmed its chemical resistance and the possibility to be used to produce leak-free FDM printed objects. Moreover, compared to commercially available VDCs (usually made with glass), the 3D printed VDCs require really low costs of production (less than 2 US $ of material) and only a few typical lab equipments such as a heating and stirring plate, a heating block and a magnetic stirring bar.

VDC *in vitro* testing results fundamental to predict results from *ex vivo* or *in vivo* studies and the possibility to have this testing system readily available in a research lab with a really low cost could increase its diffusion and utilization.

Conclusions and future outlook

CONCLUSIONS AND FUTURE OUTLOOK

3D printing has opened a new era in the pharmaceutical field. This has been possible thanks to the versatility of this innovative technology that can space from the direct production of medicines and medical devices to the production of manufacturing and analytical devices. The main strength and keyword of the 3DP is personalization. Every object created with an AM technique can be personalized based on the user's needs.

It results really helpful to produce personalized medicines and personalized devices.

In this thesis work, different applications of the FDM 3DP technique have been presented proving the high versatility of this technology with the aim to expand the knowledge about the technology.

In the close future, 3D printers specifically dedicated to the production of pharmaceutical forms will be available in the market and hopefully, they will be efficiently used in local and hospital pharmacies to formulate personalized dosage forms. Meanwhile, industrial production of a 3D printed product has already been demonstrated since 2015 when Spritam® (www.spritam.com) has been approved by FDA as the first 3D printed antiepileptic printlet. The first example of a GMP-based printer for personalized dosage forms has been already marketed by FabRX (www.fabrx.co.uk) with the name of M3DIMAKER™. All these approaches are opening the doors to 3D printing for pharmaceutical applications.

Moreover, the rapid prototyping approach could be useful at the basic research level to obtain low-cost devices such as microfluidic chips or vertical diffusion cells. This will help to widen the accessibility to different technologies around the world and increase the usage of microfluidics already from the initial research steps.

Nowadays, 3D printing is the closest technology to teleporting that we have available since it allows to exchange real objects in few second by emailing the .stl file that results printable with a regular 3D printer in every part of the world.

3D printing has revolutionized the rapid prototyping world, it is helping researchers to develop innovative ideas and it will be helpful in the future with effective applications to produce personalized medicines and devices.

References

REFERENCES

[1] J. Goole, K. Amighi, 3D printing in pharmaceutics: A new tool for designing customized drug delivery systems, Int. J. Pharm. 499 (2016) 376–394. https://doi.org/10.1016/j.ijpharm.2015.12.071.

[2] H. Ragelle, S. Rahimian, E.A. Guzzi, P.D. Westenskow, M.W. Tibbitt, G. Schwach, R. Langer, Additive manufacturing in drug delivery: innovative drug product design and opportunities for industrial application, Adv. Drug Deliv. Rev. 178 (2021) 113990. https://doi.org/10.1016/j.addr.2021.113990.

[3] D. Dimitrov, K. Schreve, N. De Beer, Advances in three dimensional printing – state of the art and future perspectives, Rapid Prototyp. J. 12 (2006) 136–147. https://doi.org/10.1108/13552540610670717.

[4] A. Melocchi, M. Uboldi, M. Cerea, A. Foppoli, A. Maroni, S. Moutaharrik, L. Palugan, L. Zema, A. Gazzaniga, A Graphical Review on the Escalation of Fused Deposition Modeling (FDM) 3D Printing in the Pharmaceutical Field, J. Pharm. Sci. 109 (2020) 2943–2957. https://doi.org/10.1016/j.xphs.2020.07.011.

[5] M. Elbadawi, L.E. McCoubrey, F.K.H. Gavins, J.J. Ong, A. Goyanes, S. Gaisford, A.W. Basit, Harnessing artificial intelligence for the next generation of 3D printed medicines, Adv. Drug Deliv. Rev. 175 (2021) 113805. https://doi.org/10.1016/j.addr.2021.05.015.

[6] S. Trenfield, A. Basit, A. Goyanes, INNOVATIONS IN 3D: Printed pharmaceuticals, ONdrugDelivery. 2020 (2020) 45–49.

[7] M. Tiboni, R. Campana, E. Frangipani, L. Casettari, 3D printed clotrimazole intravaginal ring for the treatment of recurrent vaginal candidiasis, Int. J. Pharm. (2021) 120290. https://doi.org/10.1016/j.ijpharm.2021.120290.

[8] M. Tiboni, S. Benedetti, A. Skouras, G. Curzi, D. Romano Perinelli, G. Filippo Palmieri, L. Casettari, D.R.D.R. Perinelli, G.F.G.F. Palmieri, L. Casettari, 3D-printed microfluidic chip for the preparation of glycyrrhetinic acid-loaded ethanolic liposomes, Int. J. Pharm. 584 (2020) 119436. https://doi.org/10.1016/j.ijpharm.2020.119436.

[9] M. Tiboni, M. Tiboni, A. Pierro, M. Del Papa, S. Sparaventi, M. Cespi, L. Casettari, Microfluidics for nanomedicines manufacturing: An affordable and low-cost 3D printing approach, Int. J. Pharm. 599 (2021) 120464. https://doi.org/10.1016/j.ijpharm.2021.120464.

[10] A.J.L. Morgan, L. Hidalgo San Jose, W.D. Jamieson, J.M. Wymant, B. Song, P. Stephens, D.A. Barrow, O.K. Castell, Simple and Versatile 3D Printed Microfluidics Using Fused Filament Fabrication, PLoS One. 11 (2016) e0152023. https://doi.org/10.1371/journal.pone.0152023.

[11] M. Tiboni, G. Curzi, A. Aluigi, L. Casettari, An easy 3D printing approach to manufacture vertical diffusion cells for in vitro release and permeation studies, J. Drug Deliv. Sci. Technol. 65 (2021) 102661. https://doi.org/10.1016/j.jddst.2021.102661.

[12] I. Seoane-Viaño, S.J. Trenfield, A.W. Basit, A. Goyanes, Translating 3D printed pharmaceuticals: From hype to real-world clinical applications, Adv. Drug Deliv. Rev. 174 (2021) 553–575. https://doi.org/10.1016/j.addr.2021.05.003.

[13] Y. Zhang, J. Zhao, G. Yang, Y. Zhou, W. Gao, G. Wu, X. Li, C. Mao, T. Sheng, M. Zhou, Mechanical properties and degradation of drug eluted bioresorbable vascular scaffolds prepared by three-dimensional printing technology, Https://Doi.Org/10.1080/09205063.2019.1586303. 30 (2019) 547–560. https://doi.org/10.1080/09205063.2019.1586303.

[14] M.M. Benmassaoud, C. Kohama, T.W.B. Kim, J.A. Kadlowec, B. Foltiny, T. Mercurio, S.I. Ranganathan, Efficacy of eluted antibiotics through 3D printed femoral implants, Biomed. Microdevices. 21 (2019) 1–10. https://doi.org/10.1007/S10544-019-0395-8/FIGURES/10.

[15] J. Domínguez-Robles, C. Mancinelli, E. Mancuso, I. García-Romero, B.F. Gilmore, L. Casettari, E. Larrañeta, D.A. Lamprou, 3D printing of drug-loaded thermoplastic polyurethane meshes: A potential material for soft tissue reinforcement in vaginal surgery, Pharmaceutics. 12 (2020). https://doi.org/10.3390/pharmaceutics12010063.

[16] X. Farto-Vaamonde, G. Auriemma, R.P. Aquino, A. Concheiro, C. Alvarez-Lorenzo, Post-manufacture loading of filaments and 3D printed PLA scaffolds with prednisolone and dexamethasone for tissue regeneration applications, Eur. J. Pharm. Biopharm. 141 (2019) 100–110. https://doi.org/10.1016/J.EJPB.2019.05.018.

[17] P.F. Costa, A.M. Puga, L. Díaz-Gomez, A. Concheiro, D.H. Busch, C. Alvarez-Lorenzo, Additive manufacturing of scaffolds with dexamethasone controlled release for enhanced bone regeneration, Int. J. Pharm. 496 (2015) 541–550. https://doi.org/10.1016/J.IJPHARM.2015.10.055.

[18] M.A. Luzuriaga, D.R. Berry, J.C. Reagan, R.A. Smaldone, J.J. Gassensmith, Biodegradable 3D printed polymer microneedles for transdermal drug delivery, Lab Chip. 18 (2018) 1223–1230. https://doi.org/10.1039/C8LC00098K.

[19] A. Goyanes, U. Det-Amornrat, J. Wang, A.W. Basit, S. Gaisford, 3D scanning and 3D printing as innovative technologies for fabricating personalized topical drug delivery systems, J. Control. Release. 234 (2016) 41–48. https://doi.org/10.1016/J.JCONREL.2016.05.034.

[20] J. Fu, X. Yu, Y. Jin, 3D printing of vaginal rings with personalized shapes for controlled release of progesterone, Int. J. Pharm. 539 (2018) 75–82. https://doi.org/10.1016/j.ijpharm.2018.01.036.

[21] A. Melocchi, M. Uboldi, N. Inverardi, F. Briatico-Vangosa, F. Baldi, S. Pandini, G. Scalet, F. Auricchio, M. Cerea, A. Foppoli, A. Maroni, L. Zema, A. Gazzaniga, Expandable drug delivery system for gastric retention based on shape memory polymers: Development via 4D printing and extrusion, Int. J. Pharm. 571 (2019) 118700. https://doi.org/10.1016/j.ijpharm.2019.118700.

[22] A. Melocchi, M. Uboldi, M. Cerea, A. Foppoli, A. Maroni, S. Moutaharrik, L. Palugan, L. Zema, A. Gazzaniga, Shape memory materials and 4D printing in pharmaceutics, Adv. Drug Deliv. Rev. 173 (2021) 216–237. https://doi.org/10.1016/j.addr.2021.03.013.

[23] N.R. Welsh, R.K. Malcolm, B. Devlin, P. Boyd, Dapivirine-releasing vaginal rings produced by plastic freeforming additive manufacturing, Int. J. Pharm. 572 (2019) 118725. https://doi.org/10.1016/j.ijpharm.2019.118725.

[24] L. Kasper, P. Miramón, N. Jablonowski, S. Wisgott, D. Wilson, S. Brunke, B. Hube, Antifungal activity of clotrimazole against Candida albicans depends on carbon sources, growth phase and

morphology, J. Med. Microbiol. 64 (2015) 714–723. https://doi.org/10.1099/jmm.0.000082.

[25] E.N. Ringdahl, Treatment of Recurrent Vulvovaginal Candidiasis, Am. Fam. Physician. 61 (2000) 3306–3312.

[26] K. Morrow Guthrie, S. Vargas, J.G. Shaw, R.K. Rosen, J.J. van den Berg, P.F. Kiser, K. Buckheit, D. Bregman, L. Thompson, K. Jensen, T. Johnson, R.W. Buckheit, The Promise of Intravaginal Rings for Prevention: User Perceptions of Biomechanical Properties and Implications for Prevention Product Development, (2015). https://doi.org/10.1371/journal.pone.0145642.

[27] J.W. McBride, P. Boyd, N. Dias, D. Cameron, R.E. Offord, O. Hartley, V.L. Kett, R.K. Malcolm, Vaginal rings with exposed cores for sustained delivery of the HIV CCR5 inhibitor 5P12-RANTES, J. Control. Release. 298 (2019) 1–11. https://doi.org/10.1016/j.jconrel.2019.02.003.

[28] G. Verstraete, L. Vandenbussche, S. Kasmi, L. Nuhn, D. Brouckaert, J. Van Renterghem, W. Grymonpré, V. Vanhoorne, T. Coenye, B.G. De Geest, T. De Beer, J.P. Remon, C. Vervaet, Thermoplastic polyurethane-based intravaginal rings for prophylaxis and treatment of (recurrent) bacterial vaginosis, Int. J. Pharm. 529 (2017) 218–226. https://doi.org/10.1016/j.ijpharm.2017.06.076.

[29] F. Fontana, J.P. Martins, G. Torrieri, H.A. Santos, Nuts and Bolts: Microfluidics for the Production of Biomaterials, Adv. Mater. Technol. 4 (2019) 1800611. https://doi.org/10.1002/admt.201800611.

[30] J.P. Martins, G. Torrieri, H.A. Santos, The importance of microfluidics for the preparation of nanoparticles as advanced drug delivery systems, Expert Opin. Drug Deliv. 15 (2018) 469–479. https://doi.org/10.1080/17425247.2018.1446936.

[31] X. Zhao, F. Bian, L. Sun, L. Cai, L. Li, Y. Zhao, Microfluidic Generation of Nanomaterials for Biomedical Applications, Small. 16 (2020) 1901943. https://doi.org/10.1002/smll.201901943.

[32] D. Pranzo, P. Larizza, D. Filippini, G. Percoco, Extrusion-Based 3D Printing of Microfluidic Devices for Chemical and Biomedical Applications: A Topical Review, Micromachines. 9 (2018) 374. https://doi.org/10.3390/mi9080374.

[33] V. Romanov, R. Samuel, M. Chaharlang, A.R. Jafek, A. Frost, B.K. Gale, FDM 3D Printing of High-Pressure, Heat-Resistant, Transparent Microfluidic Devices, Anal. Chem. 90 (2018) 10450–10456. https://doi.org/10.1021/acs.analchem.8b02356.

[34] V. Hessel, H. Löwe, F. Schönfeld, Micromixers - A review on passive and active mixing principles, in: Chem. Eng. Sci., 2005: pp. 2479–2501. https://doi.org/10.1016/j.ces.2004.11.033.

[35] T.C. Kao, M.H. Shyu, G.C. Yen, Glycyrrhizic acid and 18β-glycyrrhetinic acid inhibit inflammation via PI3K/Akt/GSK3β signaling and glucocorticoid receptor activation, J. Agric. Food Chem. 58 (2010) 8623–8629. https://doi.org/10.1021/jf101841r.

[36] K. Pugalendi, P. Kalaiarasi, Protective effect of 18b-glycyrrhetinic acid on lipid peroxidation and antioxidant enzymes in experimental diabetes, J. Pharm. Res. 4 (2011) 107–111. http://jprsolutions.info.

[37] A.J.N. Price, A.J. Capel, R.J. Lee, P. Pradel, S.D.R. Christie, An open source toolkit for 3D

printed fluidics, J. Flow Chem. (2020) 1–15. https://doi.org/10.1007/s41981-020-00117-2.

[38] C.Y. Lee, W.T. Wang, C.C. Liu, L.M. Fu, Passive mixers in microfluidic systems: A review, Chem. Eng. J. 288 (2016) 146–160. https://doi.org/10.1016/j.cej.2015.10.122.

[39] S. Pagano, M. Coniglio, C. Valenti, M.I. Federici, G. Lombardo, S. Cianetti, L. Marinucci, Biological effects of Cannabidiol on normal human healthy cell populations: Systematic review of the literature, Biomed. Pharmacother. 132 (2020) 110728. https://doi.org/10.1016/j.biopha.2020.110728.

[40] M. Marques, C.T. Ueda, V.P. Shah, K. Derdzinski, G. Ewing, G. Flynn, H. Maibach, H. Rytting, S. Shaw, K. Thakker, A. Yacobi, Topical and transdermal drug products, Pharmacopeial Forum. 35 (2009) 750–764.

[41] B. Gonçalves, C. Ferreira, C.T. Alves, M. Henriques, J. Azeredo, S. Silva, Vulvovaginal candidiasis: Epidemiology, microbiology and risk factors, Crit. Rev. Microbiol. 42 (2016) 905–927. https://doi.org/10.3109/1040841X.2015.1091805.

[42] K. Workowski, A.B. Gail, Sexually transmitted diseases treatment guidelines - Vulvovaginal Candidiasis, 2015.

[43] H.S. Johal, T. Garg, G. Rath, A.K. Goyal, Advanced topical drug delivery system for the management of vaginal candidiasis, Drug Deliv. 23 (2016) 550–563. https://doi.org/10.3109/10717544.2014.928760.

[44] Tietz, Klein, In Vitro Methods for Evaluating Drug Release of Vaginal Ring Formulations—A Critical Review, Pharmaceutics. 11 (2019) 538. https://doi.org/10.3390/pharmaceutics11100538.

[45] D.R. Mishell, M.E. Lumkin, Contraceptive effect of varying dosages of progestogen in silastic vaginal rings., Fertil. Steril. 21 (1970) 99–103. https://doi.org/10.1016/s0015-0282(16)37333-2.

[46] L.M. Ferguson, L.C. Rohan, The importance of the vaginal delivery route for antiretrovirals in HIV prevention, Ther. Deliv. 2 (2011) 1535–1550. https://doi.org/10.4155/tde.11.126.

[47] P. Wayne, Clinical and Laboratory Standards Institute (CLSI). Reference method for broth dilution antifungal susceptibility testing of yeats. 4th Edition, CLSI standard M27, 4th Editio, 2017.

[48] R. Rastogi, J. Su, A. Mahalingam, J. Clark, S. Sung, T. Hope, P.F. Kiser, Engineering and characterization of simplified vaginal and seminal fluid simulants, Contraception. 93 (2016) 337–346. https://doi.org/10.1016/j.contraception.2015.11.008.

[49] F. Saadatfar, A. Shayanfar, E. Rahimpour, M. Barzegar-Jalali, F. Martinez, M. Bolourtchian, A. Jouyban, Measurement and correlation of clotrimazole solubility in ethanol + water mixtures at T = (293.2 to 313.2) K, J. Mol. Liq. 256 (2018) 527–532. https://doi.org/10.1016/j.molliq.2018.02.068.

[50] P. Boyd, B. Variano, P. Spence, C.F. McCoy, D.J. Murphy, Y.H. Dallal Bashi, R.K. Malcolm, In vitro release testing methods for drug-releasing vaginal rings, J. Control. Release. 313 (2019) 54–69. https://doi.org/10.1016/j.jconrel.2019.10.015.

[51] G. Verstraete, A. Samaro, W. Grymonpré, V. Vanhoorne, B. Van Snick, M.N. Boone, T. Hellemans, L. Van Hoorebeke, J.P. Remon, C. Vervaet, 3D printing of high drug loaded dosage

forms using thermoplastic polyurethanes, Int. J. Pharm. 536 (2018) 318–325. https://doi.org/10.1016/j.ijpharm.2017.12.002.

[52] R.K. Malcolm, P.J. Boyd, C.F. McCoy, D.J. Murphy, Microbicide vaginal rings: Technological challenges and clinical development, Adv. Drug Deliv. Rev. 103 (2016) 33–56. https://doi.org/10.1016/j.addr.2016.01.015.

[53] P. Garcia Ferreira, C. Guimarães de Souza Lima, L.L. Noronha, M.C. de Moraes, F. de C. da Silva, A. Lifsitch Viçosa, D. Omena Futuro, V. Francisco Ferreira, Development of a Method for the Quantification of Clotrimazole and Itraconazole and Study of Their Stability in a New Microemulsion for the Treatment of Sporotrichosis, Molecules. 24 (2019) 2333. https://doi.org/10.3390/molecules24122333.

[54] N.V. Gupta, S. Natasha, A. Getyala, R.S. Bhat, Bioadhesive vaginal tablets containing spray dried microspheres loaded with clotrimazole for treatment of vaginal Candidiasis, Acta Pharm. 63 (2013) 359–372. https://doi.org/10.2478/acph-2013-0027.

[55] A. Haryńska, I. Gubanska, J. Kucinska-Lipka, H. Janik, Fabrication and characterization of flexible medical-grade TPU filament for Fused Deposition Modeling 3DP technology, Polymers (Basel). 10 (2018). https://doi.org/10.3390/polym10121304.

[56] C.F. McCoy, B.G. Millar, D.J. Murphy, W. Blanda, B. Hansraj, B. Devlin, R.K. Malcolm, P. Boyd, Mechanical testing methods for drug-releasing vaginal rings, Int. J. Pharm. 559 (2019) 182–191. https://doi.org/10.1016/j.ijpharm.2019.01.026.

[57] R.K. Malcolm, K.L. Edwards, P. Kiser, J. Romano, T.J. Smith, Advances in microbicide vaginal rings, Antiviral Res. 88 (2010) S30–S39. https://doi.org/10.1016/j.antiviral.2010.09.003.

[58] P. Boyd, I. Major, W. Wang, C. McConville, Development of disulfiram-loaded vaginal rings for the localised treatment of cervical cancer, Eur. J. Pharm. Biopharm. 88 (2014) 945–953. https://doi.org/10.1016/j.ejpb.2014.08.002.

[59] C. McConville, J.M. Smith, C.F. McCoy, P. Srinivasan, J. Mitchell, A. Holder, R.A. Otten, S. Butera, G.F. Doncel, D.R. Friend, R.K. Malcolm, Lack of in vitro–in vivo correlation for a UC781-releasing vaginal ring in macaques, Drug Deliv. Transl. Res. 5 (2015) 27–37. https://doi.org/10.1007/s13346-015-0216-4.

[60] J. Siepmann, N.A. Peppas, Higuchi equation: Derivation, applications, use and misuse, Int. J. Pharm. 418 (2011) 6–12. https://doi.org/10.1016/j.ijpharm.2011.03.051.

[61] T. Higuchi, Rate of release of medicaments from ointment bases containing drugs in suspension, J. Pharm. Sci. 50 (1961) 874–875. https://doi.org/10.1002/jps.2600501018.

[62] K. Malcolm, D. Woolfson, J. Russell, P. Tallon, L. McAuley, D. Craig, Influence of silicone elastomer solubility and diffusivity on the in vitro release of drugs from intravaginal rings, J. Control. Release. 90 (2003) 217–225. https://doi.org/10.1016/S0168-3659(03)00178-0.

[63] D.J. Murphy, D. Desjardins, P. Boyd, N. Dereuddre-Bosquet, L. Stimmer, A. Caldwell, R. Le Grand, C. Kelly, J. van Roey, R.K. Malcolm, Impact of ring size and drug loading on the pharmacokinetics of a combination dapivirine-darunavir vaginal ring in cynomolgus macaques, Int. J. Pharm. 550 (2018) 300–308. https://doi.org/10.1016/j.ijpharm.2018.08.051.

[64] S.R. Ugaonkar, J.T. Clark, L.B. English, T.J. Johnson, K.W. Buckheit, R.J. Bahde, D.H. Appella, R.W. Buckheit, P.F. Kiser, An Intravaginal Ring for the Simultaneous Delivery of an HIV-1 Maturation Inhibitor and Reverse-Transcriptase Inhibitor for Prophylaxis of HIV Transmission, J. Pharm. Sci. 104 (2015) 3426–3439. https://doi.org/10.1002/jps.24551.

[65] M. Nagashima, Y. Yamagishi, H. Mikamo, Antifungal susceptibilities of Candida species isolated from the patients with vaginal candidiasis, J. Infect. Chemother. 22 (2016) 124–126. https://doi.org/10.1016/j.jiac.2015.08.008.

[66] G. Pastorino, L. Cornara, S. Soares, F. Rodrigues, M.B.P.P. Oliveira, Liquorice (Glycyrrhiza glabra): A phytochemical and pharmacological review, Phyther. Res. 32 (2018) 2323–2339. https://doi.org/10.1002/ptr.6178.

[67] H. Yamaguchi, T. Noshita, T. Yu, Y. Kidachi, K. Kamiie, H. Umetsu, K. Ryoyama, Novel effects of glycyrrhetinic acid on the central nervous system tumorigenic progenitor cells: Induction of actin disruption and tumor cell-selective toxicity, Eur. J. Med. Chem. 45 (2010) 2943–2948. https://doi.org/10.1016/j.ejmech.2010.03.021.

[68] C. Fiore, M. Eisenhut, R. Krausse, E. Ragazzi, D. Pellati, D. Armanini, J. Bielenberg, Antiviral effects ofGlycyrrhiza species, Phyther. Res. 22 (2008) 141–148. https://doi.org/10.1002/ptr.2295.

[69] L.R. Huang, X.J. Hao, Q.J. Li, D.P. Wang, J.X. Zhang, H. Luo, X.S. Yang, 18β-Glycyrrhetinic Acid Derivatives Possessing a Trihydroxylated A Ring Are Potent Gram-Positive Antibacterial Agents, J. Nat. Prod. 79 (2016) 721–731. https://doi.org/10.1021/acs.jnatprod.5b00641.

[70] A.M. Aly, L. Al-alousi, H.A. Salem, Licorice : A Possible Anti-inflammatory and Anti-ulcer Drug, 6 (2005).

[71] P. Kalaiarasi, K.V. Pugalendi, Antihyperglycemic effect of 18β-glycyrrhetinic acid, aglycone of glycyrrhizin, on streptozotocin-diabetic rats, Eur. J. Pharmacol. 606 (2009) 269–273. https://doi.org/10.1016/j.ejphar.2008.12.057.

[72] I. Castangia, C. Caddeo, M.L. Manca, L. Casu, A.C. Latorre, O. Díez-Sales, A. Ruiz-Saurí, G. Bacchetta, A.M. Fadda, M. Manconi, Delivery of liquorice extract by liposomes and hyalurosomes to protect the skin against oxidative stress injuries, Carbohydr. Polym. 134 (2015) 657–663. https://doi.org/10.1016/j.carbpol.2015.08.037.

[73] M. Damle, R. Mallya, Development and Evaluation of a Novel Delivery System Containing Phytophospholipid Complex for Skin Aging, AAPS PharmSciTech. 17 (2016) 607–617. https://doi.org/10.1208/s12249-015-0386-x.

[74] M. Lu, Q. Qiu, X. Luo, X. Liu, J. Sun, C. Wang, X. Lin, Y. Deng, Y. Song, Phyto-phospholipid complexes (phytosomes): A novel strategy to improve the bioavailability of active constituents, Asian J. Pharm. Sci. 14 (2019) 265–274. https://doi.org/10.1016/j.ajps.2018.05.011.

[75] C.R. Edwards, P.M. Stewart, D. Burt, L. Brett, M.A. McIntyre, W.S. Sutanto, E.R. de Kloet, C. Monder, Localisation of 11 beta-hydroxysteroid dehydrogenase--tissue specific protector of the mineralocorticoid receptor., Lancet (London, England). 2 (1988) 986–9. https://doi.org/10.1016/s0140-6736(88)90742-8.

[76] J.A. Bouwstra, P.L. Honeywell-Nguyen, G.S. Gooris, M. Ponec, Structure of the skin barrier and

its modulation by vesicular formulations, Prog. Lipid Res. 42 (2003) 1–36. https://doi.org/10.1016/S0163-7827(02)00028-0.

[77] T.W. Prow, J.E. Grice, L.L. Lin, R. Faye, M. Butler, W. Becker, E.M.T. Wurm, C. Yoong, T.A. Robertson, H.P. Soyer, M.S. Roberts, Nanoparticles and microparticles for skin drug delivery, Adv. Drug Deliv. Rev. 63 (2011) 470–491. https://doi.org/10.1016/j.addr.2011.01.012.

[78] V.P. Torchilin, Recent advances with liposomes as pharmaceutical carriers, Nat. Rev. Drug Discov. 4 (2005) 145–160. https://doi.org/10.1038/nrd1632.

[79] Y. Zhai, G. Zhai, Advances in lipid-based colloid systems as drug carrier for topic delivery, J. Control. Release. 193 (2014) 90–99. https://doi.org/10.1016/j.jconrel.2014.05.054.

[80] G. Cevc, G. Blume, Lipid vesicles penetrate into intact skin owing to the transdermal osmotic gradients and hydration force, BBA - Biomembr. 1104 (1992) 226–232. https://doi.org/10.1016/0005-2736(92)90154-E.

[81] E. Touitou, B. Godin, Enhanced skin permeation using ethosomes, in: Percutaneous Penetration Enhanc. Second Ed., CRC Press, 2005: pp. 95–108.

[82] M.M.A. Elsayed, O.Y. Abdallah, V.F. Naggar, N.M. Khalafallah, Deformable liposomes and ethosomes: Mechanism of enhanced skin delivery, Int. J. Pharm. 322 (2006) 60–66. https://doi.org/10.1016/j.ijpharm.2006.05.027.

[83] K. Sarwa, P. Suresh, M. Rudrapal, V. Verma, Penetration of Tamoxifen Citrate Loaded Ethosomes and Liposomes Across Human Skin: A Comparative Study with Confocal Laser Scanning Microscopy, Curr. Drug Deliv. 11 (2014) 332–337. https://doi.org/10.2174/15672018116661401151131 27.

[84] A. Wagner, K. Vorauer-Uhl, Liposome Technology for Industrial Purposes, J. Drug Deliv. 2011 (2011) 1–9. https://doi.org/10.1155/2011/591325.

[85] S. Batzri, E.D. Korn, Single bilayer liposomes prepared without sonication, BBA - Biomembr. 298 (1973) 1015–1019. https://doi.org/10.1016/0005-2736(73)90408-2.

[86] C. Jaafar-Maalej, C. Charcosset, H. Fessi, A new method for liposome preparation using a membrane contactor, J. Liposome Res. 21 (2011) 213–220. https://doi.org/10.3109/08982104.2010.517537.

[87] S. Joshi, M.T. Hussain, C.B. Roces, G. Anderluzzi, E. Kastner, S. Salmaso, D.J. Kirby, Y. Perrie, Microfluidics based manufacture of liposomes simultaneously entrapping hydrophilic and lipophilic drugs, Int. J. Pharm. 514 (2016) 160–168. https://doi.org/10.1016/j.ijpharm.2016.09.027.

[88] N. Bhattacharjee, A. Urrios, S. Kang, A. Folch, The upcoming 3D-printing revolution in microfluidics, Lab Chip. 16 (2016) 1720–1742. https://doi.org/10.1039/c6lc00163g.

[89] S. Grijalvo, J. Mayr, R. Eritja, D.D. Díaz, Biodegradable liposome-encapsulated hydrogels for biomedical applications: A marriage of convenience, Biomater. Sci. 4 (2016) 555–574. https://doi.org/10.1039/c5bm00481k.

[90] S. Catalani, F. Palma, S. Battistelli, B. Nuvoli, R. Galati, S. Benedetti, Reduced cell viability and apoptosis induction in human thyroid carcinoma and mesothelioma cells exposed to cidofovir,

Toxicol. Vitr. 41 (2017) 49–55. https://doi.org/10.1016/j.tiv.2017.02.008.

[91] F. Farabegoli, E.S. Scarpa, A. Frati, G. Serafini, A. Papi, E. Spisni, E. Antonini, S. Benedetti, P. Ninfali, Betalains increase vitexin-2-O-xyloside cytotoxicity in CaCo-2 cancer cells, Food Chem. 218 (2017) 356–364. https://doi.org/10.1016/j.foodchem.2016.09.112.

[92] B. Baert, J. Boonen, C. Burvenich, N. Roche, F. Stillaert, P. Blondeel, J. van Bocxlaer, B. de Spiegeleer, A new discriminative criterion for the development of franz diffusion tests for transdermal pharmaceuticals, J. Pharm. Pharm. Sci. 13 (2010) 218–230. https://doi.org/10.18433/j3ws33.

[93] L. Kaur, K. Singh, S. Paul, S. Singh, S. Singh, S.K. Jain, A Mechanistic Study to Determine the Structural Similarities Between Artificial Membrane Strat-M^{TM} and Biological Membranes and Its Application to Carry Out Skin Permeation Study of Amphotericin B Nanoformulations, AAPS PharmSciTech. 19 (2018) 1606–1624. https://doi.org/10.1208/s12249-018-0959-6.

[94] Z. Liu, F. Fontana, A. Python, J.T. Hirvonen, H.A. Santos, Microfluidics for Production of Particles: Mechanism, Methodology, and Applications, Small. (2019). https://doi.org/10.1002/smll.201904673.

[95] E.K. Sackmann, A.L. Fulton, D.J. Beebe, The present and future role of microfluidics in biomedical research, Nature. 507 (2014) 181–189. https://doi.org/10.1038/nature13118.

[96] I.T.S. Heikkinen, C. Kauppinen, Z. Liu, S.M. Asikainen, S. Spoljaric, J. V. Seppälä, H. Savin, J.M. Pearce, Chemical compatibility of fused filament fabrication-based 3-D printed components with solutions commonly used in semiconductor wet processing, Addit. Manuf. 23 (2018) 99–107. https://doi.org/10.1016/j.addma.2018.07.015.

[97] E.M. Elmowafy, M. Tiboni, M.E. Soliman, Biocompatibility, biodegradation and biomedical applications of poly(lactic acid)/poly(lactic-co-glycolic acid) micro and nanoparticles, Springer Singapore, 2019. https://doi.org/10.1007/s40005-019-00439-x.

[98] M. Kirjavainen, A. Urtti, R. Valjakka-Koskela, J. Kiesvaara, J. Mönkkönen, Liposome-skin interactions and their effects on the skin permeation of drugs, Eur. J. Pharm. Sci. 7 (1999) 279–286. https://doi.org/10.1016/S0928-0987(98)00037-2.

[99] G.M. El Maghraby, B.W. Barry, A.C. Williams, Liposomes and skin: From drug delivery to model membranes, Eur. J. Pharm. Sci. 34 (2008) 203–222. https://doi.org/10.1016/j.ejps.2008.05.002.

[100] P. Figueiredo, C. Ferro, M. Kemell, Z. Liu, A. Kiriazis, K. Lintinen, H.F. Florindo, J. Yli-Kauhaluoma, J. Hirvonen, M.A. Kostiainen, H.A. Santos, Functionalization of carboxylated lignin nanoparticles for targeted and pH-responsive delivery of anticancer drugs, Nanomedicine. 12 (2017) 2581–2596. https://doi.org/10.2217/nnm-2017-0219.

[101] P. Zhang, Y. Cao, H. Chen, B. Zhou, W. Hu, L. Zhang, Preparation and evaluation of glycyrrhetinic acid-modified and honokiol-loaded acoustic nanodroplets for targeted tumor imaging and therapy with low-boiling-point phase-change perfluorocarbon, J. Mater. Chem. B. 5 (2017) 5845. https://doi.org/10.1039/c7tb01215b.

[102] K. Takiura, S. Honda, H. Takai, M. Kii, H. Yuki, M. Yamamoto, Studies of Oligosaccharides.

XII. Hydrophilization of Glycyrrhetinic Acid by Coupling to Gentio Oligosaccharides, Chem. Pharm. Bull. 22 (1974) 1618–1623. https://doi.org/10.1248/cpb.22.1618.

[103] H. Heerklotz, The microcalorimetry of lipid membranes, J. Phys. Condens. Matter. 16 (2004) R441. https://doi.org/10.1088/0953-8984/16/15/R01.

[104] Y.-D. Dong, A.W. Dong, I. Larson, M. Rappolt, H. Amenitsch, T. Hanley, B.J. Boyd, Impurities in Commercial Phytantriol Significantly Alter Its Lyotropic Liquid-Crystalline Phase Behavior, Langmuir. 24 (2008) 6998–7003. https://doi.org/10.1021/la8005579.

[105] H. Chauhan, S. Mohapatra, D.J. Munt, S. Chandratre, A. Dash, Physical-Chemical Characterization and Formulation Considerations for Solid Lipid Nanoparticles, AAPS PharmSciTech. 17 (2016) 640–651. https://doi.org/10.1208/s12249-015-0394-x.

[106] S. Paliwal, A. Tilak, J. Sharma, V. Dave, S. Sharma, K. Verma, K. Tak, K.R. Reddy, V. Sadhu, Flurbiprofen-loaded ethanolic liposome particles for biomedical applications, J. Microbiol. Methods. 161 (2019) 18–27. https://doi.org/10.1016/j.mimet.2019.04.001.

[107] A. Praveen, M. Aqil, S.S. Imam, A. Ahad, T. Moolakkadath, F.J. Ahmad, Lamotrigine encapsulated intra-nasal nanoliposome formulation for epilepsy treatment: Formulation design, characterization and nasal toxicity study, Colloids Surfaces B Biointerfaces. 174 (2019) 553–562. https://doi.org/10.1016/j.colsurfb.2018.11.025.

[108] Elmowafy, El-Derany, Biondo, Tiboni, Casettari, Soliman, Quercetin Loaded Monolaurate Sugar Esters-Based Niosomes: Sustained Release and Mutual Antioxidant—Hepatoprotective Interplay, Pharmaceutics. 12 (2020) 143. https://doi.org/10.3390/pharmaceutics12020143.

[109] A.E. Nel, L. Mädler, D. Velegol, T. Xia, E.M.V. Hoek, P. Somasundaran, F. Klaessig, V. Castranova, M. Thompson, Understanding biophysicochemical interactions at the nano-bio interface, Nat. Mater. 8 (2009) 543–557. https://doi.org/10.1038/nmat2442.

[110] A. Albanese, P.S. Tang, W.C.W. Chan, The Effect of Nanoparticle Size, Shape, and Surface Chemistry on Biological Systems, Annu. Rev. Biomed. Eng. 14 (2012) 1–16. https://doi.org/10.1146/annurev-bioeng-071811-150124.

[111] P. Boukamp, R.T. Petrussevska, D. Breitkreutz, J. Hornung, A. Markham, N.E. Fusenig, Normal keratinization in a spontaneously immortalized aneuploid human keratinocyte cell line, J. Cell Biol. 106 (1988) 761–771. https://doi.org/10.1083/jcb.106.3.761.

[112] A. Haq, B. Goodyear, D. Ameen, V. Joshi, B. Michniak-Kohn, Strat-M® synthetic membrane: Permeability comparison to human cadaver skin, Int. J. Pharm. 547 (2018) 432–437. https://doi.org/10.1016/j.ijpharm.2018.06.012.

[113] Y. Rahimpour, Y. Javadzadeh, H. Hamishehkar, Solid lipid microparticles for enhanced dermal delivery of tetracycline HCl, Colloids Surfaces B Biointerfaces. 145 (2016) 14–20. https://doi.org/10.1016/j.colsurfb.2016.04.034.

[114] C.H. Salamanca, A. Barrera-Ocampo, J.C. Lasso, N. Camacho, C.J. Yarce, Franz diffusion cell approach for pre-formulation characterisation of ketoprofen semi-solid dosage forms, Pharmaceutics. 10 (2018) 1–10. https://doi.org/10.3390/pharmaceutics10030148.

[115] A.L.M. Ruela, E.C. Figueiredo, A.G. Perissinato, A.C.Z. Lima, M.B. Araújo, G.R. Pereira, In

vitro evaluation of transdermal Nicotine delivery systems commercially available in Brazil, Brazilian J. Pharm. Sci. 49 (2013) 579–588. https://doi.org/10.1590/S1984-82502013000300020.

[116] J.M. Metselaar, T. Lammers, Challenges in nanomedicine clinical translation, Drug Deliv. Transl. Res. 10 (2020) 721–725. https://doi.org/10.1007/s13346-020-00740-5.

[117] P.M. Valencia, O.C. Farokhzad, R. Karnik, R. Langer, Microfluidic technologies for accelerating the clinical translation of nanoparticles, Nat. Nanotechnol. 7 (2012) 623–629. https://doi.org/10.1038/nnano.2012.168.

[118] V.K. La Mer, Nucleation in Phase Transitions., Ind. Eng. Chem. 44 (1952) 1270–1277. https://doi.org/10.1021/ie50510a027.

[119] R. Daw, J. Finkelstein, Lab on a chip, Nature. 442 (2006) 367. https://doi.org/10.1038/442367a.

[120] Q. Wu, J. Liu, X. Wang, L. Feng, J. Wu, X. Zhu, W. Wen, X. Gong, Organ-on-a-chip: Recent breakthroughs and future prospects, Biomed. Eng. Online. 19 (2020). https://doi.org/10.1186/s12938-020-0752-0.

[121] L. Capretto, W. Cheng, M. Hill, X. Zhang, Micromixing within microfluidic devices, Top. Curr. Chem. 304 (2011) 27–68. https://doi.org/10.1007/128_2011_150.

[122] A.M. Tothill, M. Partridge, S.W. James, R.P. Tatam, Fabrication and optimisation of a fused filament 3D-printed microfluidic platform, J. Micromechanics Microengineering. 27 (2017) 035018. https://doi.org/10.1088/1361-6439/aa5ae3.

[123] S.A. Vasilescu, S.R. Bazaz, D. Jin, O. Shimoni, M.E. Warkiani, 3D printing enables the rapid prototyping of modular microfluidic devices for particle conjugation, Appl. Mater. Today. 20 (2020) 100726. https://doi.org/10.1016/j.apmt.2020.100726.

[124] S. Waheed, J.M. Cabot, N.P. Macdonald, T. Lewis, R.M. Guijt, B. Paull, M.C. Breadmore, 3D printed microfluidic devices: Enablers and barriers, Lab Chip. 16 (2016) 1993–2013. https://doi.org/10.1039/c6lc00284f.

[125] C.W. Hirt, B.D. Nichols, Volume of fluid (VOF) method for the dynamics of free boundaries, J. Comput. Phys. 39 (1981) 201–225. https://doi.org/10.1016/0021-9991(81)90145-5.

[126] D. Gueyffier, J. Li, A. Nadim, R. Scardovelli, S. Zaleski, Volume-of-Fluid Interface Tracking with Smoothed Surface Stress Methods for Three-Dimensional Flows, J. Comput. Phys. 152 (1999) 423–456. https://doi.org/10.1006/jcph.1998.6168.

[127] H.G. Weller, G. Tabor, H. Jasak, C. Fureby, A tensorial approach to computational continuum mechanics using object-oriented techniques, Comput. Phys. 12 (1998) 620. https://doi.org/10.1063/1.168744.

[128] P. Desir, T.Y. Chen, M. Bracconi, B. Saha, M. Maestri, D.G. Vlachos, Experiments and computations of microfluidic liquid-liquid flow patterns, React. Chem. Eng. 5 (2020) 39–50. https://doi.org/10.1039/c9re00332k.

[129] M. Trotta, E. Peira, F. Debernardi, M. Gallarate, Elastic liposomes for skin delivery of dipotassium glycyrrhizinate, Int. J. Pharm. 241 (2002) 319–327. https://doi.org/10.1016/S0378-5173(02)00266-1.

[130] M.A. Ansari, K.Y. Kim, Mixing performance of unbalanced split and recombine micromixers

with circular and rhombic sub-channels, Chem. Eng. J. 162 (2010) 760–767. https://doi.org/10.1016/j.cej.2010.05.068.

[131] G.A. Lewis, D. Mathieu, R. Phan-Tan-Luu, D. Mathieu, R. Phan-Tan-Luu, Factor influence studies, in: Pharm. Exp. Des., CRC Press, 1998: pp. 93–164. https://doi.org/10.1201/9780203508688-5.

[132] J. Antoy, A Systematic Methodology for Design of Experiments, in: Des. Exp. Eng. Sci. Second Ed., Elsevier Ltd, 2014: pp. 33–50. https://doi.org/10.1016/C2012-0-03558-2.

[133] T. Sheriff, M.J. Lin, D. Dubin, H. Khorasani, The potential role of cannabinoids in dermatology, J. Dermatolog. Treat. 31 (2020) 839–845. https://doi.org/10.1080/09546634.2019.1675854.

[134] J.A. Karas, L.J.M. Wong, O.K.A. Paulin, A.C. Mazeh, M.H. Hussein, J. Li, T. Velkov, The antimicrobial activity of cannabinoids, Antibiotics. 9 (2020) 1–10. https://doi.org/10.3390/antibiotics9070406.

[135] T.W. Klein, Cannabinoid-based drugs as anti-inflammatory therapeutics, Nat. Rev. Immunol. 5 (2005) 400–411. https://doi.org/10.1038/nri1602.

[136] Z. Ayati, J. Sarris, D. Chang, S.A. Emami, R. Rahimi, Herbal medicines and phytochemicals for obsessive–compulsive disorder, Phyther. Res. 34 (2020) 1889–1901. https://doi.org/10.1002/ptr.6656.

[137] T.D. Ngo, A. Kashani, G. Imbalzano, K.T.Q. Nguyen, D. Hui, Additive manufacturing (3D printing): A review of materials, methods, applications and challenges, Compos. Part B Eng. 143 (2018) 172–196. https://doi.org/10.1016/j.compositesb.2018.02.012.

[138] E. Mathew, G. Pitzanti, E. Larrañeta, D.A. Lamprou, Three-dimensional printing of pharmaceuticals and drug delivery devices, Pharmaceutics. 12 (2020). https://doi.org/10.3390/pharmaceutics12030266.

[139] S.H. Lim, H. Kathuria, J.J.Y. Tan, L. Kang, 3D printed drug delivery and testing systems — a passing fad or the future?, Adv. Drug Deliv. Rev. 132 (2018) 139–168. https://doi.org/10.1016/j.addr.2018.05.006.

[140] A.J. Capel, R.P. Rimington, M.P. Lewis, S.D.R. Christie, 3D printing for chemical, pharmaceutical and biological applications, Nat. Rev. Chem. 2 (2018) 422–436. https://doi.org/10.1038/s41570-018-0058-y.

[141] K.S. Boparai, R. Singh, H. Singh, Development of rapid tooling using fused deposition modeling: A review, Rapid Prototyp. J. 22 (2016) 281–299. https://doi.org/10.1108/RPJ-04-2014-0048.

[142] B.C. Sil, R.G. Belgrave, M.P. Alvarez, L. Luo, M. Cristofoli, M.R. Penny, D.J. Moore, J. Hadgraft, S.T. Hilton, M.E. Lane, 3D-Printed Franz cells – update on optimization of manufacture and evaluation, Int. J. Cosmet. Sci. 42 (2020) 415–419. https://doi.org/10.1111/ics.12618.

[143] A. Haq, M. Dorrani, B. Goodyear, V. Joshi, B. Michniak-Kohn, Membrane properties for permeability testing: Skin versus synthetic membranes, Int. J. Pharm. 539 (2018) 58–64. https://doi.org/10.1016/j.ijpharm.2018.01.029.

[144] T. Uchida, W.R. Kadhum, S. Kanai, H. Todo, T. Oshizaka, K. Sugibayashi, Prediction of skin

permeation by chemical compounds using the artificial membrane, Strat-M™, Eur. J. Pharm. Sci. 67 (2015) 113–118. https://doi.org/10.1016/j.ejps.2014.11.002.

[145] S.F. Ng, J.J. Rouse, F.D. Sanderson, G.M. Eccleston, The relevance of polymeric synthetic membranes in topical formulation assessment and drug diffusion study, Arch. Pharm. Res. 35 (2012) 579–593. https://doi.org/10.1007/s12272-012-0401-7.

[146] A. Herman, A.P. Herman, Caffeine's mechanisms of action and its cosmetic use, Skin Pharmacol. Physiol. 26 (2012) 8–14. https://doi.org/10.1159/000343174.

[147] S. Ilbasmiş Tamer, T. Değim, Passive and iontophoretic delivery of sildenafil through the skin, Fabad J. Pharm. Sci. 32 (2007) 109–119.

[148] Y.J. Jung, J.H. Yoon, N.G. Kang, S.G. Park, S.H. Jeong, Diffusion properties of different compounds across various synthetic membranes using Franz-type diffusion cells, J. Pharm. Investig. 42 (2012) 271–277. https://doi.org/10.1007/s40005-012-0040-5.

[149] J.P. Skelly, V.P. Shah, H.I. Maibach, FDA and AAPS report of the workshop on principles and practices of in vitro percutaneous penetration studies: Relevance to bioavailability and bioequivalence, Pharm. Res. 4 (1987) 265–267. https://doi.org/10.1023/a:1016428716506.

[150] S.-F. Ng, J. Rouse, D. Sanderson, G. Eccleston, A Comparative Study of Transmembrane Diffusion and Permeation of Ibuprofen across Synthetic Membranes Using Franz Diffusion Cells, Pharmaceutics. 2 (2010) 209–223. https://doi.org/10.3390/pharmaceutics2020209.

[151] C. César dos Santos Nogueira, L. Mendes Cabral, T. Cristina dos Santos, A. Marucci, F. Alhaique, L.M. Cabral, Evaluation of new polysaccharides networks for extended-release purposes: mesquite seed gum (MSG), xanthan gum and chitosan, 2003.

List of publications

LIST OF PUBLICATIONS

1. E. Elmowafy, A. Abdal-Hay, A. Skouras, **M. Tiboni**, L. Casettari, V. Guarino, Polyhydroxyalkanoate (PHA): Applications in drug delivery and tissue engineering, Expert Rev. Med. Devices. 16 (2019) 467–482. https://doi.org/10.1080/17434440.2019.1615439.
2. E.M. Elmowafy, **M. Tiboni**, M.E. Soliman, Biocompatibility, biodegradation and biomedical applications of poly(lactic acid)/poly(lactic-co-glycolic acid) micro and nanoparticles, Springer Singapore, (2019). https://doi.org/10.1007/s40005-019-00439-x.
3. N. Pippa, A. Skouras, N. Naziris, F. Biondo, **M. Tiboni**, H. Katifelis, M. Gazouli, C. Demetzos, L. Casettari, Incorporation of PEGylated δ-decalactone into lipid bilayers: thermodynamic study and chimeric liposomes development, J. Liposome Res. 0 (2019) 000. https://doi.org/10.1080/08982104.2019.1625377.
4. M. Abou-El Nour, R.A.H. Ishak, **M. Tiboni**, G. Bonacucina, M. Cespi, L. Casettari, M.E. Soliman, A.S. Geneidi, Triamcinolone acetonide-loaded PLA/PEG-PDL microparticles for effective intra-articular delivery: synthesis, optimization, in vitro and in vivo evaluation, J. Control. Release. 309 (2019) 125–144. https://doi.org/10.1016/j.jconrel.2019.07.030.
5. **M. Tiboni**, S. Benedetti, A. Skouras, G. Curzi, D.R. Perinelli, G.F. Palmieri, L. Casettari, 3D-printed microfluidic chip for the preparation of glycyrrhetinic acid-loaded ethanolic liposomes, Int. J. Pharm. 584 (2020) 119436. https://doi.org/10.1016/j.ijpharm.2020.119436.
6. S. Bertoni, A. Machness, **M. Tiboni**, R. Bártolo, H.A. Santos, Reactive oxygen species responsive nanoplatforms as smart drug delivery systems for gastrointestinal tract targeting, Biopolymers. 111 (2020) 1–14. https://doi.org/10.1002/bip.23336.
7. P. Figueiredo, A. Lepland, P. Scodeller, F. Fontana, G. Torrieri, **M. Tiboni**, M.A. Shahbazi, L. Casettari, M.A. Kostiainen, J. Hirvonen, T. Teesalu, H.A. Santos, Peptide-guided resiquimod-loaded lignin nanoparticles convert tumor-associated macrophages from M2 to M1 phenotype for enhanced chemotherapy,

Acta Biomater. (2020). https://doi.org/10.1016/j.actbio.2020.09.038.

8. M. Cespi, G. Bonacucina, **M. Tiboni**, L. Casettari, A. Cambriani, F. Fini, D.R. Perinelli, G.F. Palmieri, Insights in the rheological properties of PLGA-PEG-PLGA aqueous dispersions: Structural properties and temperature-dependent behaviour, Polymer (Guildf). (2020). https://doi.org/10.1016/j.polymer.2020.123216.
9. M.T. Hussain, **M. Tiboni**, Y. Perrie, L. Casettari, Microfluidic production of protein loaded chimeric stealth liposomes, Int. J. Pharm. 590 (2020). https://doi.org/10.1016/j.ijpharm.2020.119955.
10. R. Campana, G. Mangiaterra, **M. Tiboni**, E. Frangipani, F. Biavasco, S. Lucarini, B. Citterio, A fluorinated analogue of marine bisindole alkaloid 2,2-bis(6-bromo-1h-indol-3-yl)ethanamine as potential anti-biofilm agent and antibiotic adjuvant against staphylococcus aureus, Pharmaceuticals. 13 (2020) 1–12. https://doi.org/10.3390/ph13090210.
11. G. Guidotti, M. Soccio, T. Posati, G. Sotgiu, **M. Tiboni**, M. Barbalinardo, F. Valle, L. Casettari, R. Zamboni, N. Lotti, A. Aluigi, N. Lotti, A. Aluigi, Regenerated wool keratin-polybutylene succinate nanofibrous mats for drug delivery and cells culture, Polym. Degrad. Stab. 179 (2020) 109272. https://doi.org/10.1016/j.polymdegradstab.2020.109272.
12. Elmowafy, El-Derany, Biondo, **Tiboni**, Casettari, Soliman, Quercetin Loaded Monolaurate Sugar Esters-Based Niosomes: Sustained Release and Mutual Antioxidant—Hepatoprotective Interplay, Pharmaceutics. 12 (2020) 143. https://doi.org/10.3390/pharmaceutics12020143.
13. F. McCartney, D.R. Perinelli, **M. Tiboni**, R. Cavanagh, S. Lucarini, G. Filippo Palmieri, L. Casettari, D.J. Brayden, Permeability-enhancing effects of three laurate-disaccharide monoesters across isolated rat intestinal mucosae, Int. J. Pharm. 601 (2021) 120593. https://doi.org/10.1016/j.ijpharm.2021.120593.
14. **M. Tiboni**, M. Tiboni, A. Pierro, M. Del Papa, S. Sparaventi, M. Cespi, L. Casettari, Microfluidics for nanomedicines manufacturing: An affordable and low-cost 3D printing approach, Int. J. Pharm. 599 (2021) 120464. https://doi.org/10.1016/j.ijpharm.2021.120464.
15. G. Matacchione, F. Gurău, A. Silvestrini, **M. Tiboni**, L. Mancini, D. Valli, M.R.

Rippo, R. Recchioni, F. Marcheselli, O. Carnevali, A.D. Procopio, L. Casettari, F. Olivieri, Anti-SASP and anti-inflammatory activity of resveratrol, curcumin and β-caryophyllene association on human endothelial and monocytic cells, Biogerontology. 0 (2021). https://doi.org/10.1007/s10522-021-09915-0.

16. **M. Tiboni**, R. Campana, E. Frangipani, L. Casettari, 3D printed clotrimazole intravaginal ring for the treatment of recurrent vaginal candidiasis, Int. J. Pharm. (2021) 120290. https://doi.org/10.1016/j.ijpharm.2021.120290.
17. **M. Tiboni**, S. Coppari, L. Casettari, M. Guescini, M. Colomba, D. Fraternale, A. Gorassini, G. Verardo, S. Ramakrishna, L. Guidi, B. Di Giacomo, M. Mari, R. Molinaro, M.C. Albertini, Prunus spinosa extract loaded in biomimetic nanoparticles evokes in vitro anti-inflammatory and wound healing activities, Nanomaterials. 11 (2021) 1–14. https://doi.org/10.3390/nano11010036.
18. **M. Tiboni**, G. Curzi, A. Aluigi, L. Casettari, An easy 3D printing approach to manufacture vertical diffusion cells for in vitro release and permeation studies, J. Drug Deliv. Sci. Technol. 65 (2021) 102661. https://doi.org/10.1016/j.jddst.2021.102661.
19. **M. Tiboni**, L. Casettari, L. Illum, Nasal vaccination against SARS-CoV-2: synergistic or alternative to intramuscular vaccines?, Int. J. Pharm. (2021) 120686. https://doi.org/10.1016/j.ijpharm.2021.120686.